Air–Sea Interaction in the Ligurian Sea: Assessment of a Coupled Ocean–Atmosphere Model Using In Situ Data from LASIE07

R. J. SMALL,*,+ T. CAMPBELL,* J. TEIXEIRA,# S. CARNIEL,@ T. A. SMITH,* J. DYKES,* S. CHEN,& AND R. ALLARD*

* *Naval Research Laboratory, Stennis Space Center, Mississippi*
+ *National Center for Atmospheric Research, Boulder, Colorado*
# *National Aeronautics and Space Administration Jet Propulsion Laboratory, Pasadena, California*
@ *Consiglio Nazionale delle Ricerche, ISMAR, Castello, Venice, Italy*
& *Naval Research Laboratory, Monterey, California*

(Manuscript received 25 March 2010, in final form 25 October 2010)

ABSTRACT

In situ experimental data and numerical model results are presented for the Ligurian Sea in the northwestern Mediterranean. The Ligurian Sea Air–Sea Interaction Experiment (LASIE07) and LIGURE2007 experiments took place in June 2007. The LASIE07 and LIGURE2007 data are used to validate the Coupled Ocean–Atmosphere Mesoscale Prediction System (COAMPS)[1] developed at the Naval Research Laboratory. This system includes an atmospheric sigma coordinate, nonhydrostatic model, coupled to a hydrostatic sigma-z-level ocean model (Navy Coastal Ocean Model), using the Earth System Modeling Framework (ESMF).

A month-long simulation, which includes data assimilation in the atmosphere and full coupling, is compared against an uncoupled run where analysis SST is used for computation of the bulk fluxes. This reveals that COAMPS has reasonable skill in predicting the wind stress and surface heat fluxes at LASIE07 mooring locations in shallow and deep water. At the LASIE07 coastal site (but not at the deep site) the validation shows that the coupled model has a much smaller bias in latent heat flux, because of improvements in the SST field relative to the uncoupled model. This in turn leads to large differences in upper-ocean temperature between the coupled model and an uncoupled ocean model run.

1. Background and aims

a. Ligurian Sea: Meteorology and oceanography

The Ligurian Sea, in the northwestern Mediterranean, comprises the ocean area east of the Gulf of Lion and north of the island of Corsica (Fig. 1). The weather over the Ligurian Sea is strongly influenced by the surrounding landmasses, and in particular the mountain ranges of the Alps, Massif Central, and the Pyrenees. Cyclogenesis occurs in the lee of the Alps year-round, with a strong seasonal cycle: it is most common in winter, but still occurs in summer, when the number of low pressure systems is typically about half that which normally occurs in winter (Buzzi and Speranza 1983).

In the situation of a low centered in the Gulf of Genoa, synoptic northerly flow impinges on the mountain ranges, and is funneled by the topography, leading to strong topographic jets, the northerly Mistral flowing between the Alps and Massif Central and down the Rhine valley, and the northwesterly Tramontane between the Massif Central and the Pyrenees (e.g., Flamant 2003). Although the Mistral and Tramontane events are better known for their impact in winter (Schott et al. 1996), they also occur in the summer, as documented by Drobinski et al. (2005).

In summer, the mean wind picture [Fig. 2a, from the Quick Scatterometer (QuikSCAT)] shows the influence of the Mistral and Tramontane winds, with strong northwesterly winds emanating from the Gulf of Lion, curving cyclonically in the Ligurian Sea to southwesterly in the Gulf of Genoa. Winds are weaker in the Gulf of Genoa and in the lee of the islands of Corsica and Sardinia, whereas a strong corner jet exists at the northwest tip of

[1] COAMPS is a registered trademark of the Naval Research Laboratory.

Corresponding author address: R. J. Small, National Center for Atmospheric Research, 1850 Table Mesa Dr., Boulder, CO 80305. E-mail: jsmall@ucar.edu

DOI: 10.1175/2010MWR3431.1

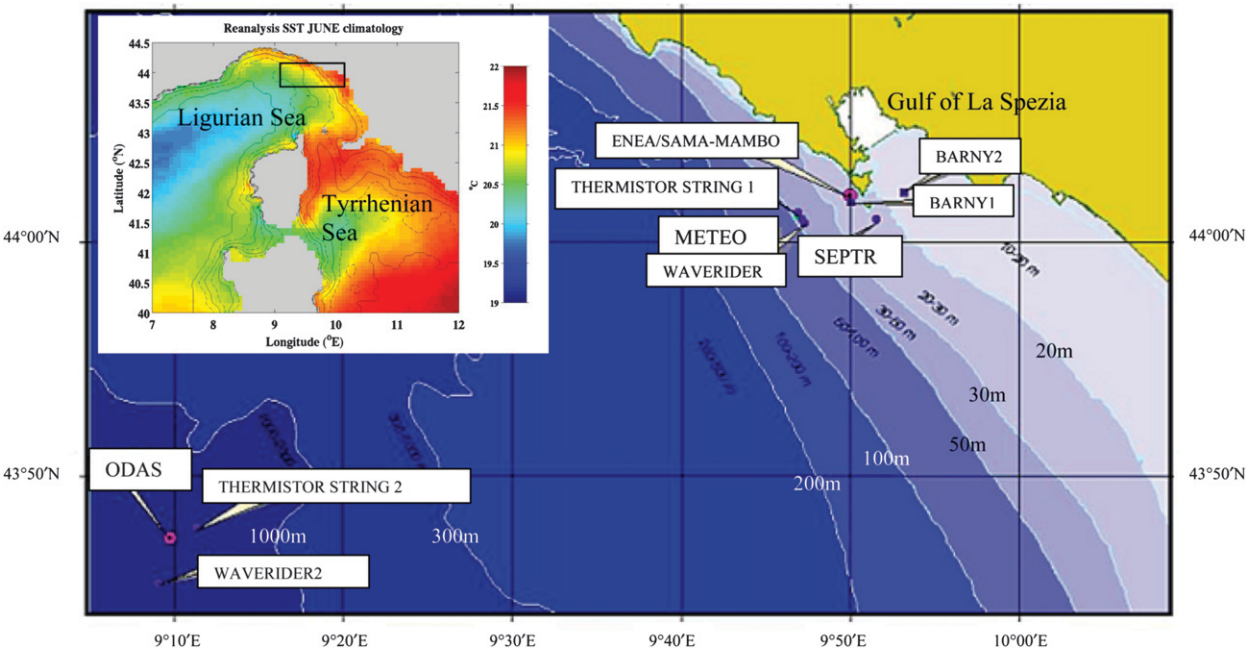

FIG. 1. Location of LASIE07. The inset shows climatological mean SST in June, and the bathymetry, for the Ligurian and Tyrrhenian Sea. SST is obtained from the GOS CNR reanalysis products (Marullo et al. 2007). Bathymetry is contoured at 2000, 500, and 100 m (solid), and 1000, 200, and 50 m (dashed). The outlined rectangle is shown in detail in the large map indicating the LASIE07 instrument positions and bathymetry, adapted from Teixeira (2007). Here the ODAS spar buoy, the METEO meteorological buoy, and the SEPTR profiling instrument are the main sources of validation data used in this study. Other instruments included thermistor strings, Waverider wave buoys, a combined current and thermistor mooring (ENEA/SAMA-MAMBO), and ADCPs (BARNY).

Corsica, and there is a jet in the Strait of Bonifacio between the two islands (see Fig. 2a for locations). The latter has been observed and noted by previous investigators [e.g., Salusti (1998) shows an example where a jet with instantaneous wind speed up to 10 m s^{-1} was observed in the strait during a Mistral ''burst'' in October 1989] and is important to the ocean circulation (Astraldi and Gasparini 1994).

A basin-scale cyclonic ocean circulation characterizes the Ligurian Sea (Crépon et al. 1982) with strong currents around its edge: including the westward Liguro-Provencal or Northern Current flowing close to the southern European coast and the west Corsica Current (Astraldi and Gasparini 1992). This cyclonic gyre has been attributed to geostrophic adjustment to winter deep-water formation (Crépon et al. 1989) and the influence of cyclonic wind stress curl east of the axis of the Mistral (Herbaut et al. 1997). The climatology of SST for June (Fig. 1, inset) shows relatively cool SST associated with strong wind stress and the doming up of cold dense waters in the Ligurian Sea gyre, and cool SST east of the Strait of Bonifacio, where winds are strong. Warmer SST is found in the shallow coastal regions with a frontal region separating the deep and shallow zones, which is particularly notable south and east of the Gulf of Genoa, where the experiment described in section 2a took place.

Previous modeling studies of the Ligurian Sea region have included ocean general circulation models focused on operational and multimodel approaches (e.g., Onken et al. 2005) or on nesting capabilities (Barth et al. 2005). As discussed below, air–sea interaction is important in the region and necessitates the use of an interactive, coupled ocean–atmosphere model, which, to the best of our knowledge, has not been done before in this region. At time of press we became aware of the coupled model studies of Somot et al. (2008) and Artale et al. (2010) for the whole Mediterranean basin.

b. *Aims of this study*

The aims of this study are twofold. First we wish to validate a two-way coupled model against a detailed dataset of atmospheric and oceanic measurements. Second we will investigate the feedbacks from the ocean in the Ligurian Sea, using fully coupled simulations and an uncoupled system where the atmospheric model receives no feedback from the ocean model. This paper is aimed toward the evaluation of the model for possible future operational use. In that context the coupled model is compared against existing regional model systems operated by the U.S. Navy, such as the Coupled Ocean–Atmosphere Mesoscale Prediction System (COAMPS) run in atmosphere-only mode, and the Navy Coastal

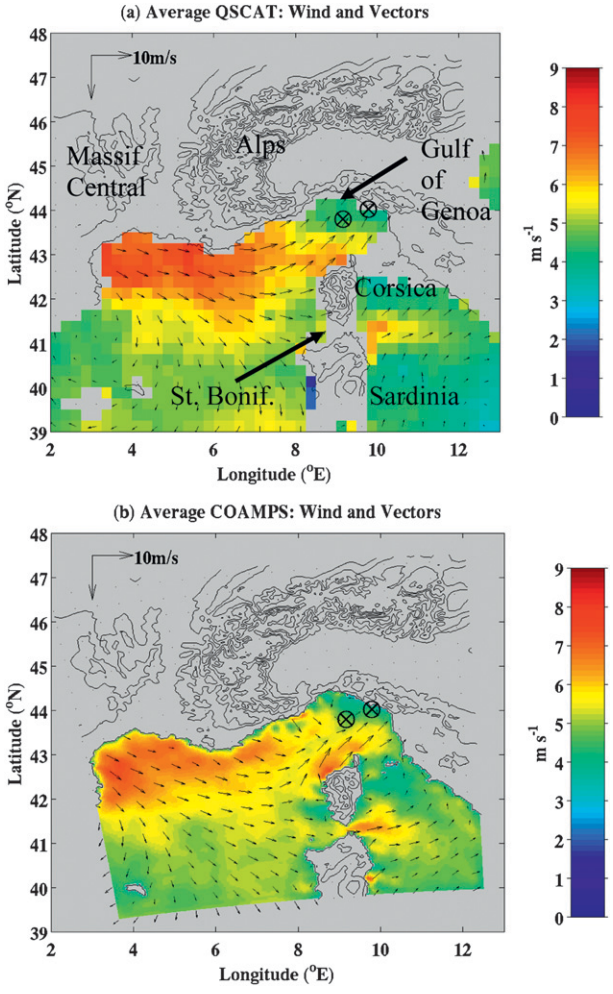

FIG. 2. Near-surface winds over Ligurian Sea. (a) Monthly average of neutral-equivalent 10-m winds from QuikSCAT. (b) Monthly average of 10-m winds from COAMPS, coupled run, inner 4-km grid. The data are averaged from 10 Jun to 9 Jul 2007, using model data only at times of the QuikSCAT swath (0600 and 1800 LT). The topography used in the atmospheric 4-km grid is contoured at 500-m intervals. The location of the ODAS (offshore) and METEO (coastal) moorings are shown in circles. In (a) the locations of the Alps, Massif Central, Gulf of Genoa, Corsica, Sardinia and the Strait of Bonifacio (St. Bonif.) are marked.

Ocean Model (NCOM) model (these models and analyses are described in section 2b). The approach used here is similar to that of Pullen et al. (2007), who studied Bora processes in the Northern Adriatic Sea using an earlier version of the model with a coarser (1 h) coupling interval.

The paper is structured as follows. Section 2 introduces the experimental dataset and the model. Section 3 provides an overview of the wind and sea level pressure fields from observations and model to set the scene. Sections 4 and 5 validate the surface and near-surface variables, and the fluxes, from the model against the observations at a deep-water site and a shallow-water site, respectively. In section 6 the mechanisms responsible for differences between the coupled and uncoupled runs are detailed. This is followed by the conclusions.

2. Observations and models

a. LASIE-07 AND LIGURE2007 experiment

A field experiment to study air–sea interaction processes in the Ligurian Sea [Ligurian Sea Air–Sea Interaction Experiment 2007 (LASIE07) for location see Fig. 1] took place in June 2007. This was a multi-institutional experiment led by the North Atlantic Treaty Organization (NATO) Undersea Research Centre (NURC).[2] During a concurrent experiment LIGURE2007, the Institute of Marine Science of the Italian Consiglio Nazionale delle Richerche (CNR-ISMAR) coordinated the Research Vessel (R/V) *Urania* during the period 17–22 June (Carniel et al. 2010, hereafter C10). The focus of the experiments was on the ocean and atmosphere boundary layers, to provide an ideal test bed with which to evaluate coupled models and boundary layer parameterizations. Full details of the experimental plan are contained in Teixeira (2007) and Sempreviva et al. (2010) and C10 present analysis of some of the datasets.

The model validation in this paper is primarily against data from two buoys: (i) the Meteorological (METEO) buoy in a total water depth of 44 m, and (ii) the permanent Ocean Data Acquisition System (ODAS) buoy where the water depth is 1333 m (for locations see Fig. 1). Note that LASIE07 in situ data were not assimilated into COAMPS, and thus represent an independent dataset for validation. On the ODAS mooring, there are measurements of wind, air temperature and relative humidity, solar radiation, and downwelling longwave radiation at a height of about 14.5 m and atmospheric pressure at 8 m (Sempreviva et al. 2010). In addition, a subsurface thermistor string measured ocean temperature at 1-, 12-, and 28-m depth. ODAS recorded data at 0.2 Hz but we use 3-h averages. The METEO buoy recorded wind speed, air temperature and humidity at a height of about 2.5 m above the surface, and the data used here are 1-h averages. In the text, the deep-water experiment region will also be referred to as the ODAS region, and similarly METEO will be used to refer to the coastal region.

Near-surface ocean temperature data are also obtained from in situ profiles. Turbulence microstructure probe data were acquired from R/V *Urania* while the ship was drifting with the engine switched off, positioned at the ODAS buoy as starting point. The probe was deployed

[2] A full list of participants is given in Teixeira (2007).

for multiple profiles (''a series''), each profile lasting about 15 min, with 6–8 profiles per series, and the data were further averaged into mean values for each of these series (C10). In addition the Shallow-water Environmental Profiler in Trawl-safe, Real-time configuration (SEPTR), provided data near the METEO location. SEPTR consists of a bottom-mounted ADCP with an additional autonomous profiling instrument, which rises to the surface about once every 4 h (and transmits data via satellite communication) and then descends (Grandi et al. 2005). Data are used from the descending portion, which takes just a few minutes in water depths of 20–30 m. The instruments include a conductivity–temperature–depth (CTD) probe to measure profiles of temperature and salinity.

b. COAMPS numerical model

Numerical simulations are performed with COAMPS, developed at the Naval Research Laboratory (NRL). The atmospheric component is a terrain-following sigma coordinate, nonhydrostatic model (Hodur 1997; Chen et al. 2003). There are three nests of horizontal spacing 36, 12, and 4 km, respectively (see Fig. 3 for the nest locations). The ocean component is the hydrostatic NCOM, which uses a combination of terrain-following sigma and z-level coordinates (Martin 2000; Martin et al. 2006). The ocean model was set up with an outer and inner nest with 6- and 2-km grid spacing, respectively (see Fig. 3). Time steps for the outer ocean and atmospheric grids are both 90 s. Details of the numerical schemes of these models can be found in the above-mentioned references, while some of the most important schemes for this study are listed in Table 1, along with details of the vertical discretization. Initial and boundary conditions for both models are also listed in Table 1.

Atmospheric data assimilation comprises creating a new initial, analyzed field every 12 h, at 0000 and 1200 UTC every day (Hodur 1997; Chen et al. 2003, 2010). The model is then run forward for 12 h in hindcast mode, and then the cycle is repeated. For the ocean model, there is no data assimilation or analysis performed; thus, the ocean component is a continuous month-long simulation constrained only by the initial, surface, and lateral boundary conditions.

The models are coupled using the Earth System Modeling Framework (ESMF, see online at http://www.earthsystemmodeling.org/). At every coupling interval (12 min here), the uppermost gridcell temperature from the ocean model (located at 0.25-m depth in our experiments, here representing the SST), along with the lowest model level atmospheric variables (temperature, humidity, wind velocity, pressure, and radiative fluxes), are used to compute the bulk fluxes, with the Coupled Ocean–Atmosphere Response Experiment, version 3

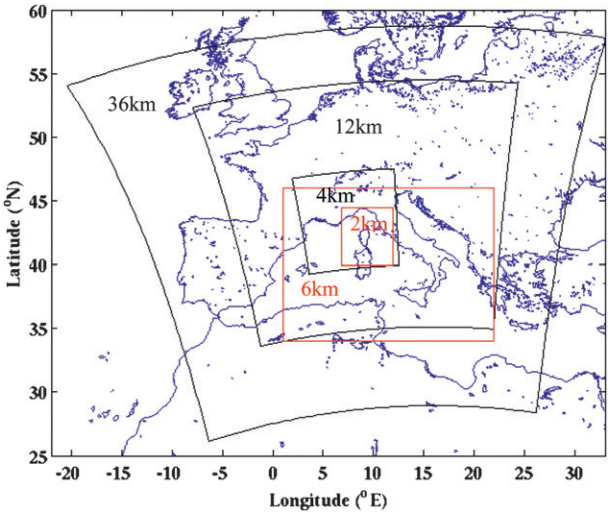

FIG. 3. Map showing model nests for the atmosphere (in black) and ocean (red). The corresponding grid resolutions are annotated.

(COARE 3.0) scheme (Fairall et al. 2003). No correction is made for the diurnal warm layer or cool skin effect (Fairall et al. 1996b)—the importance of this is discussed further in section 4c. Over land, the fluxes are computed using an updated version of the Louis (1979) scheme (Chen et al. 2003).

The model is initialized on 10 June, 5 days before the main observation–model comparison begins. Because of the lack of data assimilation in the ocean model, a short spinup is used to avoid too much drift of the ocean model from observed conditions.

c. General Ocean Turbulence Model

To understand more fully the coupled model simulations of SST, one-dimensional (1D) ocean mixed layer simulations have been performed. We compared two of the turbulence schemes in the General Ocean Turbulence Model (GOTM; see online at http://www.gotm.net/; Burchard et al. 1999; Umlauf and Burchard 2003) suite, namely the k–ε (Rodi 1987) and the Mellor–Yamada level-2.5 closure (MY2.5; Mellor and Yamada 1982). The latter scheme is also used in the NCOM model. For the experiments below, the simulations from these two techniques yielded results that were within 0.2°C, and we only show results from the k–ε model.

The simulations were initialized using a LASIE07 CTD profile from 17 June taken close to ODAS. The 1D model was discretized with a 0.5-m vertical grid to a maximum depth of 50 m. In the main experiment, the 1D model was forced with the observed wind velocity, air temperature, relative humidity, longwave and shortwave radiation, and pressure (this set of variables is referred to here as ''atmospheric forcing''), from the ODAS meteorological

TABLE 1. List of physical schemes, vertical coordinates, and boundary and initial conditions for (a) the atmospheric model and (b) the ocean model.

(a) Atmosphere

Physical process	Scheme	Reference	Comments
Grid-resolved moist processes	Single-moment bulk prediction	Rutledge and Hobbs (1983)	Many updates, see Hodur (1997); Chen et al. (2003)
Subgrid-scale convection	Kain–Fritsch	Kain and Fritsch (1993)	Switched on when grid resolution is >10km: otherwise explicit (above)
Mixing	Vertical: 2.5-level turbulence closure	Mellor and Yamada (1982)	Prognostic equation for TKE, diagnostic for fluxes of heat, moisture, momentum
	Horizontal: Fourth order	Hodur (1997); Chen et al. (2003)	
Surface layer over ocean	Bulk scheme	Land: Louis (1979) Ocean: Fairall et al. (2003)	Updated to include saturation of drag coefficient at high winds (Powell et al. 2003)
Radiation	Multiband	Harshvardhan et al. (1987)	4 bands for longwave, 5 bands for shortwave
Grid and vertical levels	Arakawa C-grid. Sigma-z coordinate to ~31-km height	Hodur (1997); Chen et al. (2003)	40 vertical layers (with 14 layers in the lowest 1000 m, and four in the lowest 100 m)
Initial and boundary conditions source	NOGAPS 1° output	Hogan and Rosmond (1991)	Boundary conditions are 6-hourly. NOGAPS is a global spectral, data assimilating system. See Hodur (1997) for description of boundary condition schemes.
Nesting and map projection	Lambert conformal, multiple nests	Hodur (1997); Chen et al. (2003)	The model configuration used here does not provide feedback from inner nests to the outer nests

(b) Ocean

Physical process	Scheme	Reference	Comments
Mixing	Vertical: 2.5-level turbulence closure	Mellor and Yamada (1982), Large et al. (1994)	Prognostic equation for TKE, diagnostic for fluxes of heat, moisture, momentum. Modified to include mixing by unresolved processes at Richardson numbers <0.7.
	Horizontal: Smagorinsky horizontal diffusion	Smagorinsky (1963)	
Tides	Tidal potential included		Tidal potential from the Oregon State University Tidal Database for K1, O1, P1, Q1, K2, M2, N2, S2, MF, and MM
Solar absorption	Jerlov-type Ia solar extinction profile	Paulson and Simpson (1977)	
Grid and vertical levels	Arakawa C-grid. Terrain-following sigma and z-level coordinates. Includes a free surface (the sigma coordinates move up and down with the surface elevation)	Martin (2000); Barron et al. (2006)	In deep water (>550 m) there are typically 10 layers in the top 10 m, and 24 in the top 100 m, allowing for good resolution of upper-ocean processes (in shallower water, the resolution increases as dictated by the sigma coordinates).
Initial and boundary conditions source	Global, data assimilating version of the NCOM, 1/8 degree model	Barron et al. (2006)	Boundary conditions are 6-hourly. Orlanski (1976) radiation boundary conditions [except Flather and Proctor (1983) for elevation and depth-average normal velocity].
Nesting and map projection	Multiple nests, spherical projection	Similar to atmospheric model (Hodur 1997; Chen et al. 2003)	The model configuration used here does not provide feedback from inner nests to the outer nests

instruments. The fluxes forcing the 1D model are therefore computed using these values and the modeled SST.

d. Satellite data

Equivalent neutral wind vectors at 10 m (Wentz and Smith 1999) are derived from the SeaWinds QuikSCAT scatterometer and obtained from the Remote Sensing Systems Web site (http://www.remss.com/). The twice-daily [approximately 0600 and 1800 local time (LT)] data are mapped onto a regular Cartesian ¼° grid.

To aid the SST validation, we use an optimal interpolation of infrared satellite SST provided by the Gruppo di Oceanografia da Satellite (GOS) group at CNR's Istituto di Scienze dell'Atmosfera e del Clima (ISAC) in Rome, Italy (GOS-CNR, Marullo et al. 2007). For analysis of SST at the coastal METEO site, we also use a higher-resolution, 2-km gridded level 4 (L4) data from the Medspiration project, associated with the Global Ocean Data Assimilation Experiment (GODAE) High-Resolution Sea Surface Temperature group. (Further information can be found online at http://www.medspiration.org/products/.)

e. COAMPS model experiments and validation approach

The main experiment comprises a pair of numerical simulations for a 1-month period. The first run is a fully coupled (also referred to as two-way coupled) run using the model as described above in section 2b, which will be referred to as the coupled atmosphere–ocean (CAO) run. For the second simulation, we run the atmosphere and ocean components, but now the SST from the ocean is not passed to the atmosphere. Instead the atmospheric model uses SST from an analysis of observations [i.e., Navy Coupled Ocean Data Assimilation (NCODA); Cummings 2005] to compute the bulk fluxes. The NCODA SST analysis mainly uses Advanced Very High Resolution Radiometer multichannel satellite SST data, processed onto a 4-km grid (May et al. 1998), and corrected to show a subsurface or "bulk" SST (Barron and Kara 2006), as well as in situ ship and buoy data gathered within ±3 h of analysis time. The NCODA analysis is performed during the model run every 12 h on the model grid scale (e.g., 4 km here for the inner atmospheric nest). These fluxes are then used within the atmosphere and ocean model. We refer to the atmospheric portion of this system, together with the bulk fluxes, as the uncoupled atmosphere (UA) run and the ocean component as uncoupled ocean (UO). All runs employ data assimilation in the atmosphere but not the ocean.

For the model validation, the general philosophy was to use the nearest model output height (or depth) to the available observations. For example, ODAS meteorological measurements were mostly at 14.5 m and the nearest model output height was 10 m, while METEO meteorological measurements were at 2.5 m and the nearest model output height was 2 m. The model data we use are instantaneous output at mostly 1-h intervals (subsurface ocean variables were at every 3 h). For comparison with the ODAS meteorological data, averages of 3-hourly instantaneous values are used. All model–data comparisons are done for the innermost model nest [i.e., the 4-km nest for the atmosphere (and bulk fluxes), and the 2-km nest for subsurface ocean quantities].

3. Validation of wind fields and sea level pressure

Before performing detailed validations at the deep and shallow sites, we set the scene by describing the typical wind and sea level pressure conditions in the region using data from satellite scatterometer and the ODAS and METEO moorings, compared to COAMPS simulations.

Typically, near-surface wind speeds in the LASIE07 trial area were light, with a monthly average about 4 to 5 m s^{-1} (Fig. 2a, see location of circles). The COAMPS winds from the CAO run (Fig. 2b), are similar in overall structure to QuikSCAT (Fig. 2a), and include significant detail and fine structure (e.g., the jet through the Strait of Bonifacio mentioned in section 1). A slight low bias of about 1 m s^{-1} in model wind speed in the Gulf of Lions can be seen. [Note that QuikSCAT data are not assimilated into this COAMPS run; however, some satellite wind information was obtained from the Special Sensor Microwave Imager (SSM/I) satellites.]

The sea level pressure record at the ODAS buoy provides a summary of the synoptic variability during and just after the LASIE07 experiment. Three major low pressure systems occurred during 24–28 June, 1–5 July, and 8–11 July (Fig. 4a, black line), with pressure drops of about 10 hPa. Smaller low pressure signals occurred during 22–23 June and at the beginning of record (15 June). Time series of the wind vectors at the same location (Figs. 4b–d) confirmed that winds strengthened during the aforementioned low pressure systems and were directed to the north and east, and these were associated with Mistral winds off the Gulf of Lion. Observed wind speeds reached 10 m s^{-1} or more during these 5 synoptic events (Fig. 5a, black line) with a peak value of 15 m s^{-1} at the end of the day on 3 July.

The COAMPS model tracks the low pressure variations very well (Fig. 4a, blue and red lines for CAO and UA, respectively), and has a reasonable representation of the synoptic variability of wind speed (Fig. 5a) and direction (Figs. 4b–d). The overall correlation for 10-m wind speed between the CAO run and observation at ODAS is 0.60 from 3-hourly averages. The correlation of the CAO run at ODAS is significant at 99%, using the

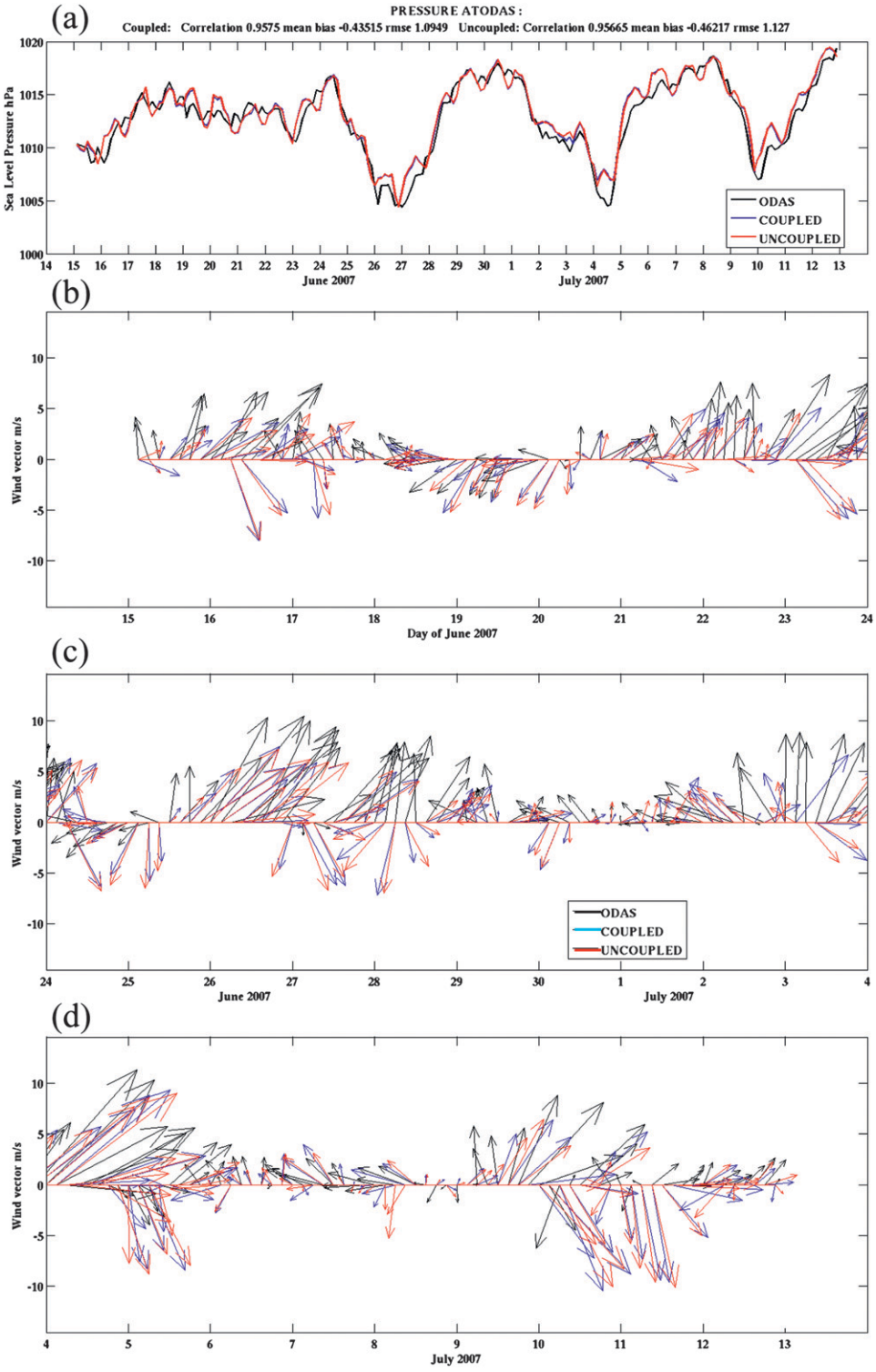

FIG. 4. (a) Sea level pressure at the ODAS mooring (black) and in the coupled (CAO) and uncoupled (UA) models (see the legend), as a function of time during the LASIE07 experiment. The corresponding wind vector time series for (b) 15–23 Jun, (c) 24 Jun–3 Jul, (d) 4–12 Jul [see legend in (c)]. Model data are from the COAMPS inner (4 km) grid, nearest grid point to the observation site. In (a), the correlation coefficient between model and observation, mean bias (observed minus model), and rmse are given in the plot subtitle, for the (left) coupled and (right) uncoupled run.

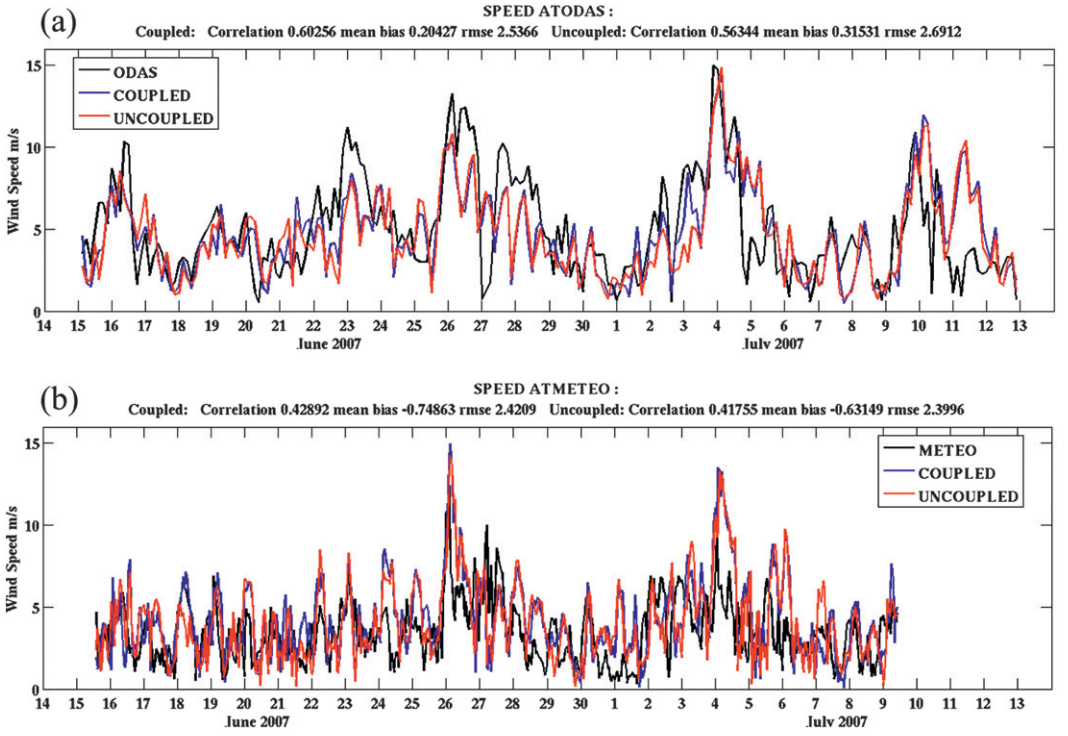

FIG. 5. (a) Wind speed measurements from LASIE07 mooring data and from COAMPS. Observations (black lines) from the ODAS buoy. Model data from COAMPS inner (4 km) grid, nearest the grid point, 10-m wind: coupled (CAO, blue) and uncoupled (UA, red). COAMPS hourly data are averaged onto the 3-h-average period of ODAS. (b) Wind speed comparison for observations from the METEO buoy and the COAMPS model. Here hourly averages of METEO data are compared against hourly outputs from the model. In this and many of the subsequent time series plots, the correlation coefficient between model and observation, mean bias (observed minus model), and rmse are given in the plot subtitle, for the (left) coupled and (right) uncoupled run (see Table 2).

Student's *t* test, under the assumption that an independent sample length is about 1 day (confirmed by autocorrelation plots). The mean bias (observed minus model) is small, 0.2 m s^{-1}, but it is clear from Fig. 5a that differences can be large in individual wind events, as evidenced by an rmse of 2.54 m s^{-1} (Table 2a gives further statistics of the model–observation comparison).

Transient variability of the winds from the METEO buoy is seen in Fig. 5b. The observed wind speeds approached 10 m s^{-1} or more on 26–27 June and 3–4 July events. The overall correlation between the CAO run and observation at the METEO buoy is 0.43, from hourly data, significant at 95% (Table 2b). The mean bias is −0.74 m s^{-1} while the rmse is 2.40 m s^{-1}, similar to that at ODAS. It can be noted that the COAMPS model produces a strong wind in the morning at METEO (Fig. 5b), which is less prominent and more irregular in the observations, suggestive of a land–sea-breeze error. A comparison with QuikSCAT swath data, detailed in Allard et al. (2010), confirmed that the diurnal variation of the wind in COAMPS is much too large, by a factor of 2–3, especially in the region of the Gulf of Genoa where LASIE07 took place. This may be due to warmer SST in the model with respect to the data, which would exaggerate the land breeze but diminish the sea breeze.

The UA run (red line in Figs. 4 and 5) produces similar wind speeds to those in the CAO run (blues lines in the corresponding figures), but has slightly lower correlations: 0.56 and 0.42 at ODAS and METEO, respectively, while the mean bias and rmse values are comparable to the coupled case (Table 2). The differences in correlation between the CAO and UA wind speeds are not significant at 95%, using a standard two-tailed Fisher-*z* approach, at both the deep and shallow site. Similarly, for the turbulent heat flux correlations and radiative fluxes at the deep site, the correlations are not significantly different between the runs (section 4). It will be shown below (section 5) that the largest differences are obtained at the coastal site.

4. Model validation at a deep-water site

Here we compare the COAMPS simulations with data from the deep water (ODAS) site. To compute the

TABLE 2. COAMPS inner grid validation against LASIE07 data. The columns show correlation coefficient (cc), mean bias (mb, observed minus model), and rmse for the coupled model (CAO) and uncoupled model (UA). (a) Validation at ODAS buoy for 15 Jun–12 Jul 2007 and (b) at METEO buoy. Wind speed statistics for the METEO buoy are for 15 Jun–9 Jul, while the statistics of air temperature, relative humidity, wind stress, and sensible heat fluxes at METEO are derived for 15–26 Jun.

	cc		mb		rmse	
(a) ODAS buoy	CAO	UA	CAO	UA	CAO	UA
Wind stress (N m^{-2})	0.69	0.68	0.0005	0.0026	0.0498	0.0519
Wind speed (m s^{-1})	0.60	0.56	0.20	0.32	2.54	2.69
Downwelling solar flux (W m^{-2})	0.94	0.94	−15.94	−19.06	121.3	115.6
Longwave radiation (W m^{-2})	0.63	0.64	−2.75	−1.97	24.28	24.20
Near-surface air temperature (°C)	0.62	0.59	−0.17	0.16	1.01	1.02
Near-surface relative humidity (%)	0.65	0.67	3.31	2.13	8.52	9.40
Sensible heat flux (W m^{-2})	0.53	0.40	−3.99	−3.88	6.73	8.48
Latent heat flux (W m^{-2})	0.58	0.61	−30.62	−25.91	42.25	56.94
	cc		mb		rmse	
(b) METEO buoy	CAO	UA	CAO	UA	CAO	UA
Wind speed (m s^{-1})	0.43	0.42	−0.74	−0.63	2.40	2.40
Wind stress (N m^{-2})	0.34	0.29	−0.007	−0.004	0.02	0.05
Near-surface air temperature (°C)	0.50	0.09	1.13	2.05	3.12	2.76
Near-surface relative humidity (%)	0.54	0.50	−6.79	−6.69	11.80	11.92
Sensible heat flux (W m^{-2})	0.61	0.57	−4.27	2.79	6.49	9.05
Latent heat flux (W m^{-2})	0.72	0.76	−4.29	25.55	39.90	47.24

observed bulk fluxes, the wind measurements, air temperature and humidity from the ODAS mooring are used, together with the ODAS ocean temperature at 1-m depth, in the Fairall et al. (1996a, 2003) COARE3.0 algorithm.

a. Radiation

Downwelling solar irradiances from ODAS and COAMPS are presented in Fig. 6a. Agreement is very good on the clear-sky days, which leads to the overall high correlation of 0.94 for both the CAO and UA runs, respectively (Table 2). However, on nonclear-sky days, agreement is not as good (e.g., COAMPS significantly overpredicts the solar flux on 18–22 June), and the rmse is quite large, around 120 W m^{-2} in both simulations. The virtual agreement of the CAO and UA runs (most of the time these curves appear to overlay) show that coupled processes do not play a significant role in changing the amount of incoming radiation, at least in this particular case.

The net longwave radiation (Fig. 6b) shows similar multiday trends in model and observations, explaining the high correlations (0.63 in CAO, 0.64 in UA, see Table 2a), and the small mean bias (less than 3 W m^{-2}), but there are large differences on subdaily time scales, so that the rmse is 24 W m^{-2} for both runs. During days when clouds are present in the model boundary layer (e.g., the 16, 17, 21, and 22 June) the net longwave drops toward zero in the morning both in model and observations (see Fig. 6b). Ceilometer measurements from R/V *Urania* confirmed the presence of clouds below 2000 m on these days (Sempreviva et al. 2010).

b. Sea surface temperature

Time series of near-surface ocean temperature from the ODAS mooring, from the CAO run, and from the NCODA analysis used to compute fluxes in the UA run are shown in Fig. 7a. In this summertime situation with strong solar insolation (Fig. 6a) and frequent occurrence of light winds below 5 m s^{-1} (Fig. 5a), diurnal warm layer effects can be expected (Fairall et al. 1996b). In Fig. 7a model data are taken from a model level at 1.1-m depth, to be consistent with the ODAS 1-m temperature data. The NCODA value represents the bulk SST: in its standard configuration used here, using bulk-corrected satellite data (see section 2d), and with the 12-h update cycle, it is not designed to represent diurnal warming (J. Cummings 2009, personal communication; see also Reynolds and Chelton 2010).

The CAO results (blue line) show similar trends to the observations (shown as black dots and connected dots), with cycles of warming and cooling over several day periods (i.e., atmospheric synoptic time scales) being comparable (Fig. 7a). However, two features are immediately obvious: 1) the CAO results appear to produce a stronger diurnal cycle of SST on some days, and 2) a bias of generally warmer temperature occurs after 20 June, and is at least 1°C too warm after 26 June (10 days into the run: the first 5 days are not shown). These two issues will be addressed in turn.

1) DIURNAL CYCLE

Regarding the diurnal cycle difference between model and observations, unfortunately the near-surface

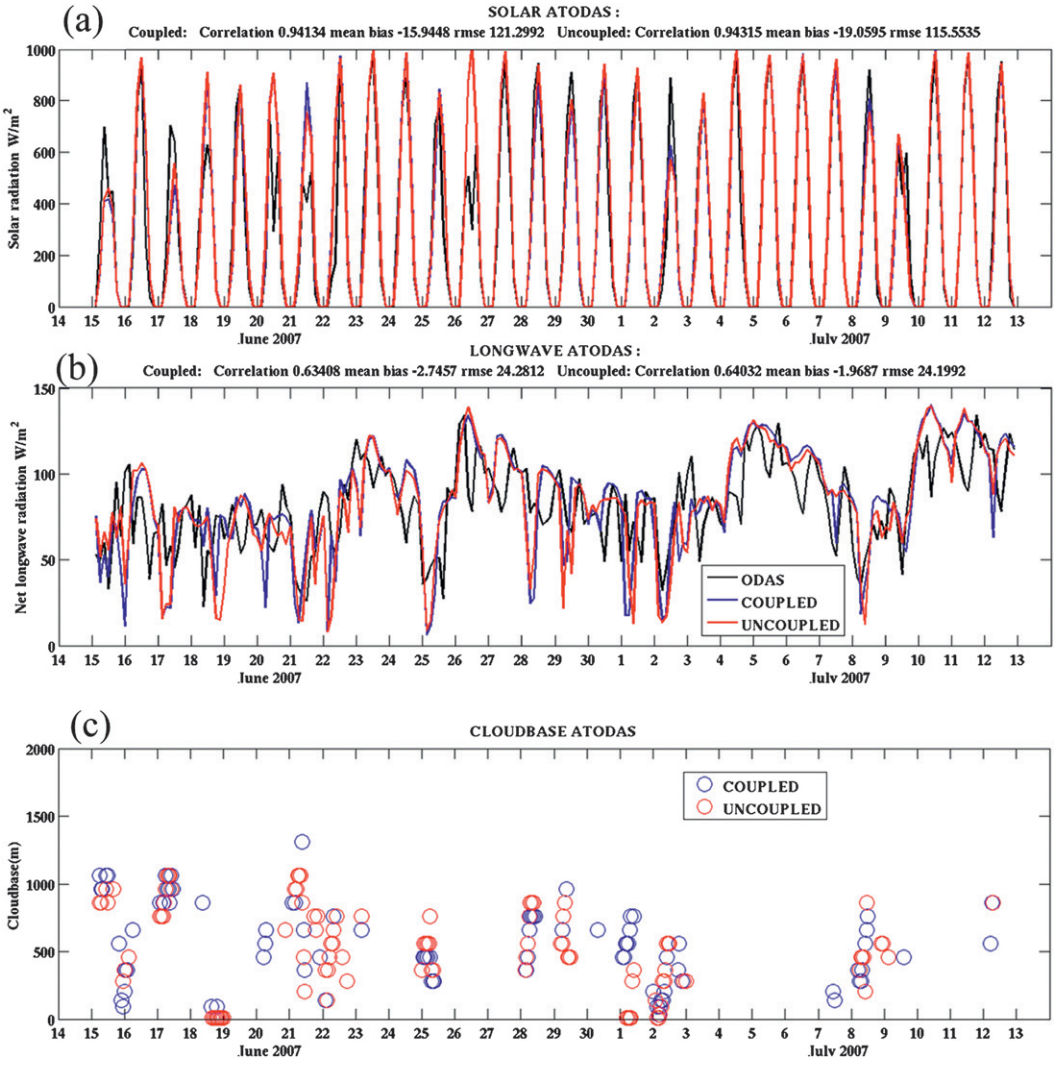

FIG. 6. (a) As in Fig. 5, but for downwelling solar flux measurements from LASIE07 mooring data and from COAMPS. (b) As in Fig. 5, but for longwave radiation. The ODAS downwelling measurements are subtracted from an estimate of upwelling IR, given by $\varepsilon\sigma T^4$, where ε is the emissivity of seawater (set to 0.98 here), σ is the Steffan–Boltzmann constant, and T is surface temperature, estimated here by the 1-m ocean temperature (which here is linearly interpolated in time across data gaps). (c) Cloud base from the COAMPS CAO and UA runs. Only cloud bases less than 2000 m are shown here.

temperature dataset from ODAS had several gaps (Fig. 7a), as well as 3-h averaging, both of which degrade an analysis of the diurnal cycle. Therefore, to help identify whether the mean bias and diurnal cycle difference between model and observation is due to model error or drift of the instrumental readings or both, we compared an independent dataset. Here we use data from the free-falling turbulence microstructure probe deployed from R/V *Urania* (C10). The mean temperature values at 2 m (temperatures closer than 2 m to the surface are not reliable because of intrinsic limitation of this technique) are shown in Fig. 7a as a green line (data cover 17–20 June only). A diurnal cycle is clear in the observations, of amplitude (i.e., maximum evening temperature minus minimum morning temperature) of up to 0.75°C at 2-m depth.

More detailed information on the performance of the coupled model in representing the near-surface and diurnal cycle can be found by showing the vertical temperature structure. The temperature at 2, 3, and 4 m from the turbulence probe (Fig. 8a) is compared against those at 1, 2, 3, and 4 m from the CAO run (Fig. 8b). The diurnal range at 2 m in the model and observations is comparable (0.5°–1°C). The temperatures at 2, 3, and 4 m in the observations collapse onto the same value each day just before sunrise: this value is the ''foundation SST''

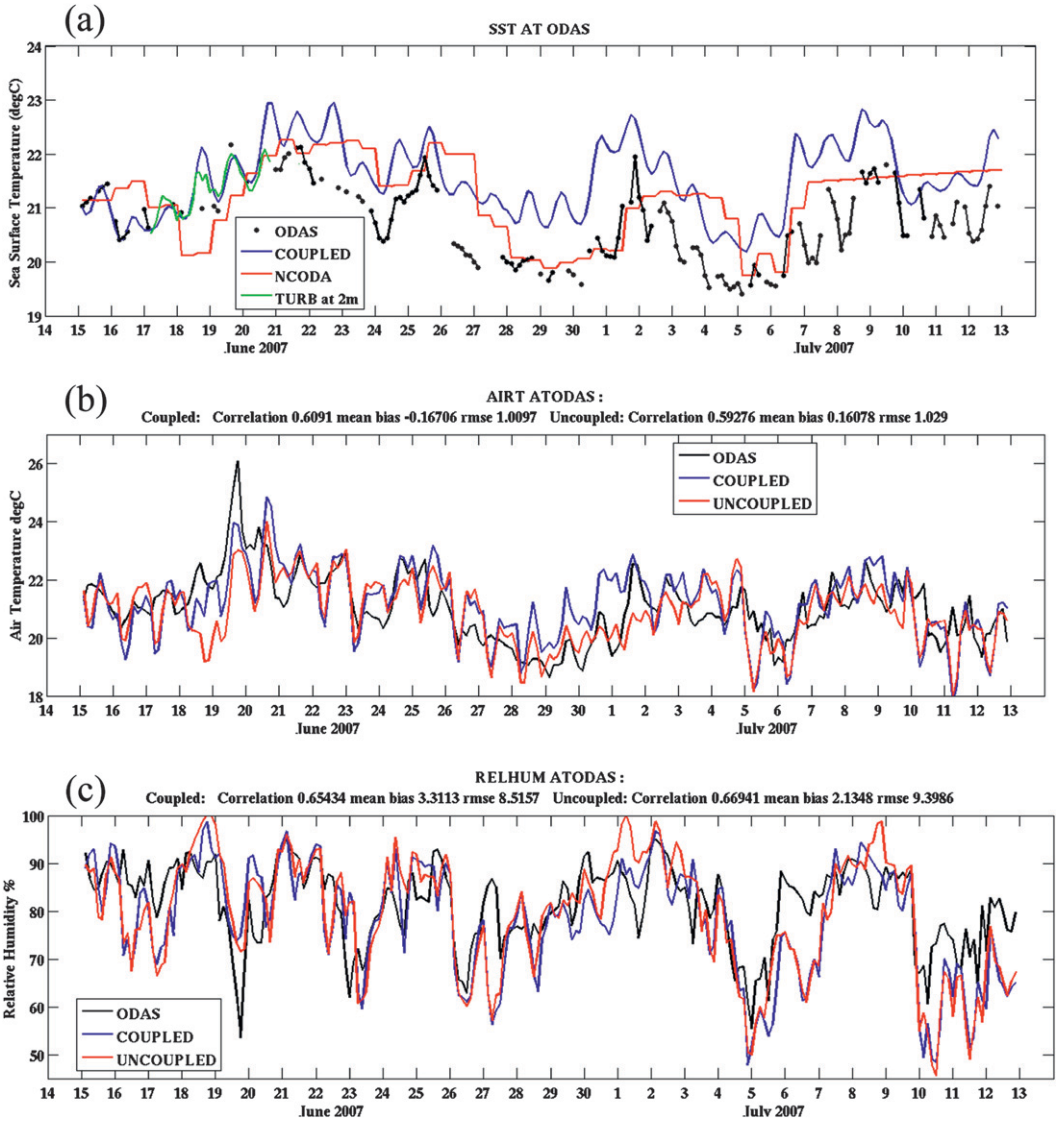

FIG. 7. As in Fig. 5, but for (a) SST, (b) near-surface air temperature, and (c) near-surface relative humidity at ODAS. In (a) the curves show (see the legend) the ODAS 1-m ocean temperature, the corresponding 1-m temperature from the fully coupled run, the NCODA SST used for the atmospheric model in the uncoupled run, and 2-m temperatures derived from turbulence probe data. In (b) and (c) model data are at 10 m and observed relative humidity and air temperature are at 14.5 m.

(defined as the temperature at the first time of the day when the heat gain from the solar radiation absorption exceeds the heat loss at the sea surface, see the Group for High Resolution SST Web site online at http://www.ghrsst.org/SST-Definitions.html). However, the model is more stratified than the observations, both in the daytime, and at night, such that the 2-, 3-, and 4-m temperatures do not return to the foundation temperature. (There is also evidence of nondiurnal, possibly internal wave effects influencing the 4-m model record, e.g., at day 20.25, Fig. 8b.) Inspection of a longer record of the CAO ocean temperatures (not shown) revealed that this was not a systematic problem with the model simulation: from 22 June onward, the top 4-m temperatures do collapse onto the foundation temperature.[3]

An important question arises as to whether the temperature at 1-m depth is a suitable quantity here for representing SST in the computation of surface fluxes from bulk algorithms. Following Price et al. (1986) and

[3] A possible reason for the change at around 22 June is that the nighttime latent heat flux is nearly zero in the period before 22 June in the model, and gets larger thereafter, which should lead to more buoyant convection after 22 June.

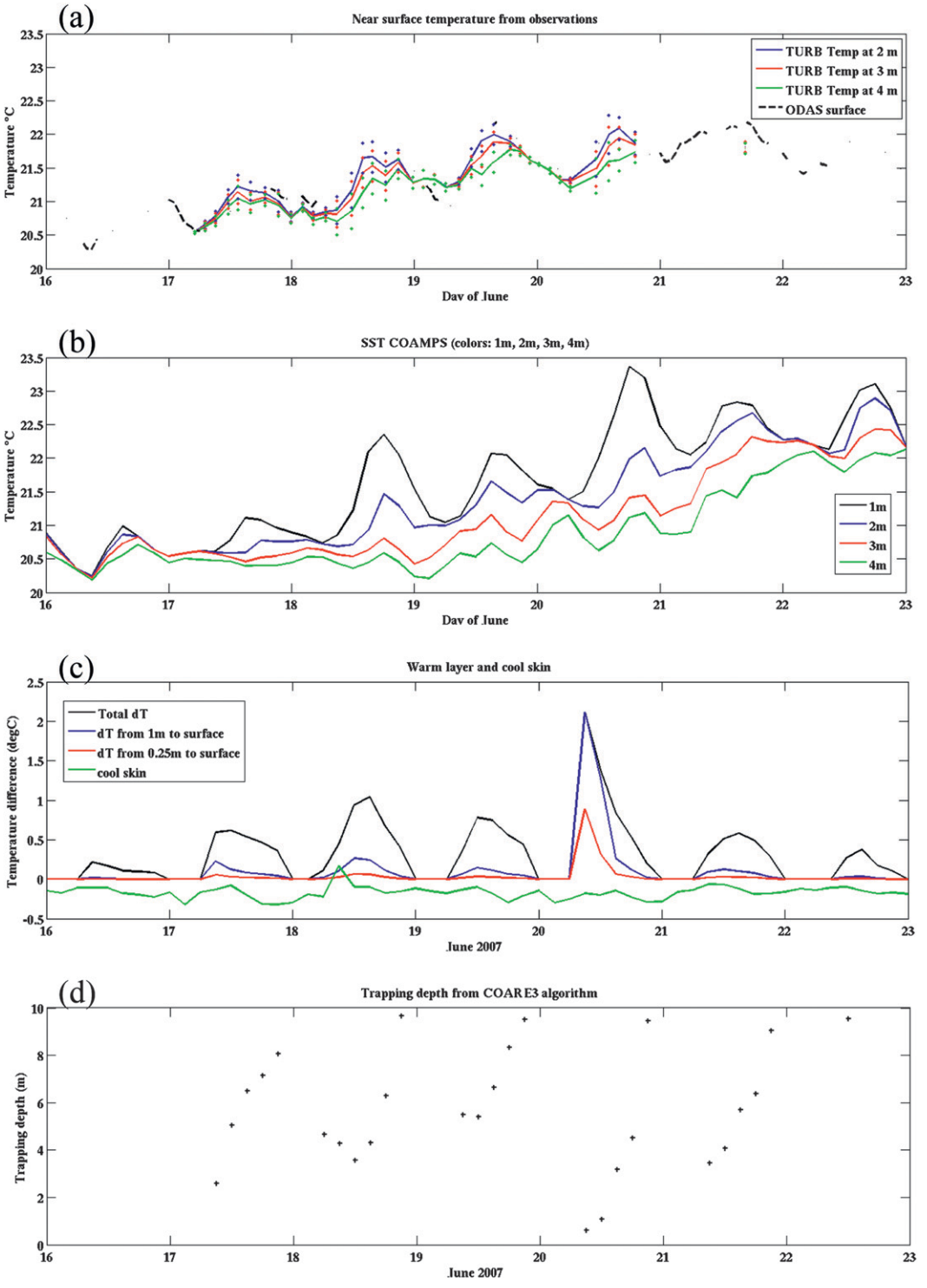

FIG. 8. SST diurnal cycle near ODAS. (a) Near-surface temperature data from turbulence microstructure probes (thick solid lines and small colored dots) deployed from RV *Urania*, and original ODAS data (blue dashed line). The thick solid lines denote mean values from a series of casts, with different colors denoting different depths (see the legend), while the ± 1 standard deviation is shown as small colored dots. (b) The near-surface temperatures from the NCOM component of the coupled model. Different colors denote different depth cells, as noted in the legend. (c) Expected properties of the diurnal warm layer and cool skin, using the COARE3.0 algorithm, with observed ODAS fluxes. The curves show the temperature difference due to diurnal warming at various depths (see text) and due to the cool skin effect. (d) The COARE3.0 predicted trapping depth of the diurnal heating.

Fairall et al. (1996b), the diurnal warm layer and cool skin effect are estimated from the COARE3.0 algorithm, using the meteorological data from ODAS. Later this will be used to see whether the bulk fluxes at ODAS are sensitive to the inclusion of skin temperature rather than 1-m ocean temperature. Figure 8d shows the expected trapping depth of solar radiation (Price et al. 1986) for a time period corresponding to Figs. 8a,b. Figure 8c shows the predicted diurnal warming and cool skin: the black line is total diurnal temperature increase from the trapping depth to the surface: the blue and red lines are the temperature change from 1 m to the surface, and from 0.25 m to the surface, respectively: and the green line is the longwave (skin) cooling. So, for example, on 18 June the trapping depth is about 4 m in the afternoon, and the total temperature change due to diurnal warming is about 1°C. This amplitude and depth of penetration is reasonably consistent with the observed temperature structure in Fig. 8a. The COAMPS model has a larger diurnal cycle on 18 June (1.5°C): possibly because the model downwelling short wave radiation is more than observed (Fig. 6a). On 20 June the predicted trapping depth is 1 m or less (Fig. 8d) and the diurnal warming amplitude 2°C. This is somewhat consistent with the large warming at 1 m at COAMPS (Fig. 8b), but the turbulence data suggest a deeper trapping depth (Fig. 8a).

2) MEAN SST BIAS BETWEEN CAO MODEL AND ODAS

The mean bias in SST initially appears to get large from 26 June onward (Fig. 7a). As shown in Figs. 5a and 6a, 26 June was a day of strong winds and cloud cover, which were both underestimated by COAMPS. The relative importance of these two factors was explored with the help of a 1D k–ε mixed layer model (section 2c) to interpret the observed and fully 3D model results. Figure 9a shows time series of upper-layer temperature from the 1D model. With surface forcing taken from the ODAS data, the temperature drops just below 21°C between 26 and 28 June, in response to the strong winds (Fig. 9a, black line). Next, sensitivity studies were done of the effect of different surface forcings (i.e., the meteorological variables). If the observed winds used to compute the surface fluxes are replaced by winds from the CAO run (and all other meteorological variables left the same), the cooling is reduced by about1°C (Fig. 9a, blue line). In contrast, if just the observed radiation used as forcing is replaced with that from CAO, there are some differences in the diurnal cycle (e.g., 20 and 21 June), but the mean bias is not significantly affected (Fig. 9a, red line). This suggests that underestimation of wind speed is the major surface forcing factor in the warm bias in the CAO run.

When the 1D mixed layer simulation with observed ODAS forcing is compared with the actual ODAS temperature and turbulence profiler temperatures (Fig. 9b) it can be seen that the mixed layer model does well initially, but also develops a warm bias of around 1°C, part of which is most likely due to a lack of advective processes, although deficiencies in the model representation of mixing cannot be ruled out. Comparing the results of the full CAO simulation against the mixed layer simulation with CAO surface fluxes further reveals a difference of about 1°C (Fig. 9c, blue solid and dashed lines). As the mixed layer model gives similar results to the MY2.5 scheme (Table 1) used in the ocean part of the coupled model, these differences must be mostly due to missing advection terms in the 1D model approach.[4]

c. Near-surface temperature, humidity, and surface turbulent fluxes

Both the near-surface air temperature and near-surface relative humidity in the CAO and UA runs are well correlated (0.6 or above, Table 2a) with the ODAS observations (Figs. 7b,c) but, as with the wind speeds, there are significant differences on daily and subdaily scales, so that the rmse are around 1°C for air temperature and 9% for relative humidity, in both runs. For example, large-amplitude cold, dry intrusions often occur in the early morning in both the CAO and UA runs, while these are absent or weak in the observations (e.g., 16, 17, 20, and 22 June). Analysis of vertical profiles from the model and from radiosonde data (Sempreviva et al. 2010) revealed that the oscillations are related to the land–sea-breeze error discussed above, such that in the early morning cold and dry air from the high landmass to the east is advected over the mooring location in the model (Allard et al. 2010). These errors, when combined with the general tendency for the coupled model SST to be too high (Fig. 7a), lead to large sea–air temperature and air–sea specific humidity difference, and consequently overlarge sensible and latent heat fluxes on those days (Figs. 10a,b).

The latent heat flux plot (Fig. 10b) shows that the model has some skill in reproducing some of the large 150–200 W m^{-2} events that occur on the strong wind days of 23 and 26 June, and early on 4 July (note that the data gaps in the observed fluxes correspond to missing ODAS 1-m ocean temperature), and the modeled sensible heat flux also matches well the observations during large amplitude events such as 4 and 9 July. As expected, the wind stress (Fig. 10c) tends to exaggerate the model–observation differences seen in the wind speed during

[4] An ocean heat budget of a short simulation similar to CAO showed that horizontal advection and vertical mixing made similar contributions to the mixed layer cooling at ODAS.

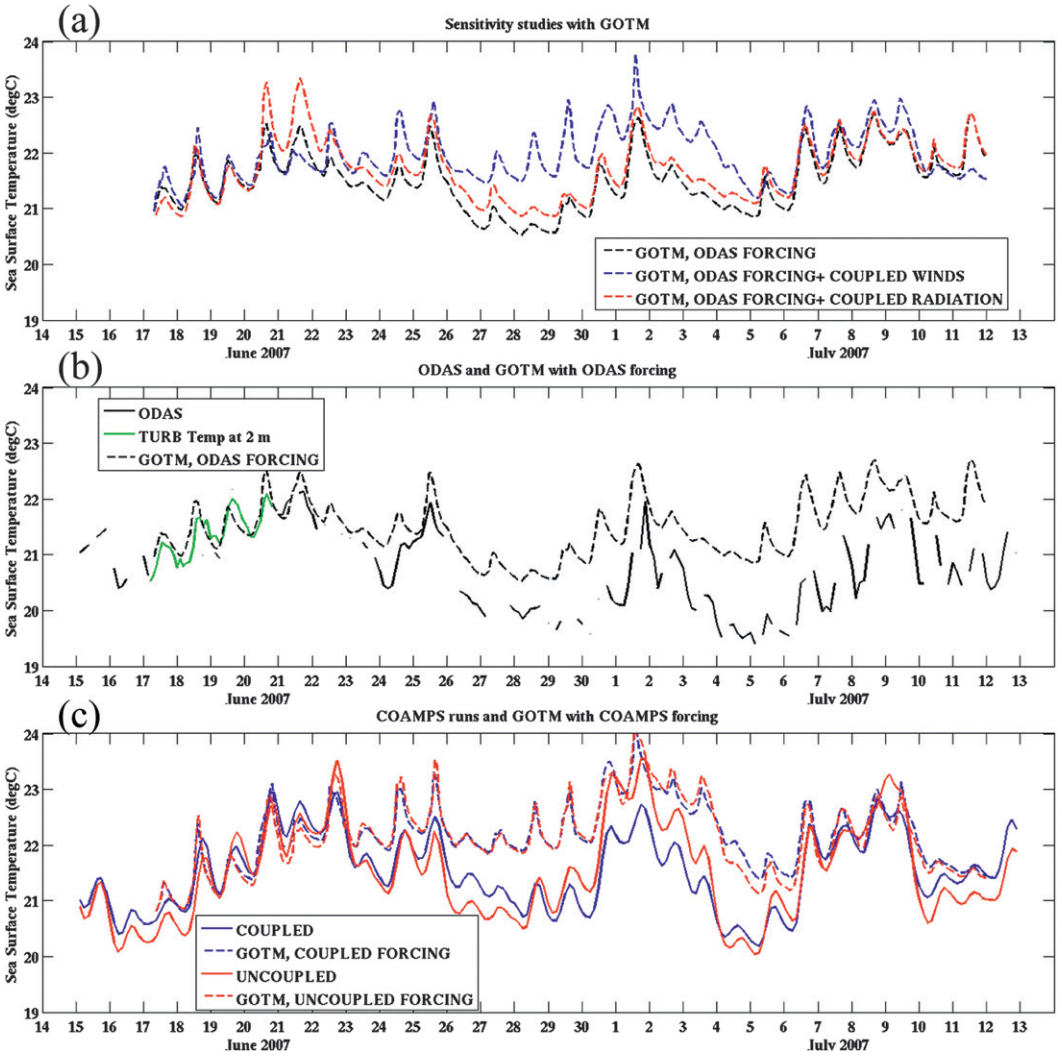

FIG. 9. Time evolution of near surface temperature "SST" from ODAS, the COAMPS model, and GOTM (k–ε) model. (a) The GOTM model with forcing from ODAS (black) is compared to sensitivity tests (i) with ODAS forcing except for winds, which are from the coupled model (blue), and (ii) with ODAS forcing except for radiation (shortwave and longwave), which are from the coupled model (red). (b) ODAS 1-m temperature and 1-m temperature from the GOTM model with ODAS surface forcing. (c) The coupled and uncoupled COAMPS model results (solid lines) and GOTM runs using forcing from the corresponding COAMPS model (dashed lines). The k–ε model gives very similar results to MY2.5, which is used in NCOM.

strong winds (e.g., on 23 and 26 June; Fig. 5a). Despite these aforementioned weaknesses of the model, the correlation coefficient between the CAO run and observations are high: 0.69 for wind stress, 0.53 for sensible heat flux, and 0.58 for latent heat flux, all significant at 99% (Table 2a). The mean bias for latent heat flux and sensible heat flux are -31 and -4 W m^{-2}, respectively, while the rmse are 42 and 7 W m^{-2}, respectively (Table 2a). The corresponding correlation coefficients for the UA run are 0.68, 0.40, and 0.61 for stress, sensible heat flux, and latent heat flux, respectively (Table 2a); the differences between coupled and uncoupled correlations are not significant. In addition, although the mean bias in latent heat flux is smaller in the UA run, the rmse is larger (Table 2a).

The results above do not include the effect of the diurnal warm layer and cool skin shown in Figs. 8c,d. The sensitivity of the heat fluxes to these effects is shown in Fig. 10d. Differences in ODAS observed heat fluxes computed with and without the cool skin/warm layer are generally very small, (e.g., less than 1 W m^{-2} for sensible heat and 5 W m^{-2} for latent heat) except during 5 of the largest-amplitude diurnal warming events during the month, where differences can be up to 10 W m^{-2} in

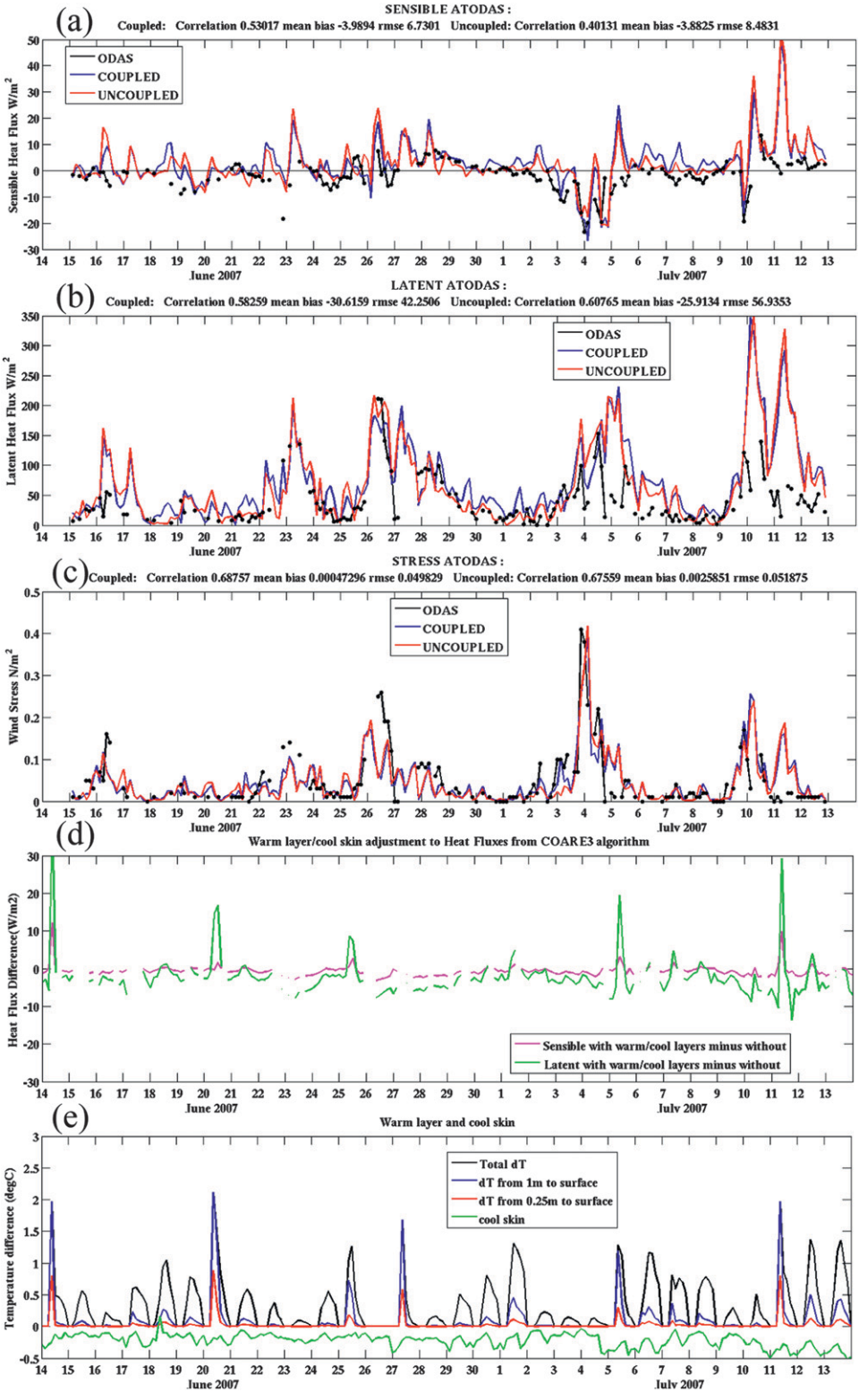

FIG. 10. As in Fig. 5, but for (a) sensible heat flux, (b) latent heat flux, and (c) wind stress at ODAS. (d) The adjustment to sensible heat flux and latent heat flux (see the legend) due to the inclusion of the diurnal warm layer and cool skin in the bulk fluxes. (e) As in Fig. 8c, but for a longer time record.

sensible heat flux and 30 W m^{-2} in latent heat flux. As seen from Fig. 10e, (an extended version of Fig. 8c), the diurnal temperature change from 1 m to surface (blue line) is generally small (due either to cloud cover reducing the incoming shortwave radiation (Fig. 6a), and/or moderate to strong winds (Fig. 5a) leading to a deep trapping depth (Fig. 8c) and compensated by the cool skin, except during the above-mentioned 5 events (note the effect of the large expected diurnal warming on 27 June is not seen in the bulk fluxes because of a data gap in 1-m ODAS temperature). Finally, we may mention that corresponding adjustments for the cool skin or warm layer for the COAMPS temperature at 0.25 m (the upper model level taken to represent SST), will be much smaller than those for the 1-m ODAS temperature (cf. the results for 0.25 and 1 m in Fig. 10e). Hence, the resulting change of surface model heat fluxes due to these diurnal effects would be considerably less than those for the observations in Fig. 10d.

5. Model validation at the shallow-water site

In addition to the deep water ODAS site, fluxes have been estimated for the location of the METEO buoy, in shallow water (Fig. 1). Unfortunately no coincident SST data were available from the buoy and for this reason we use near-surface temperature measurements from the nearby SEPTR instrument, located in 24.5-m-deep water (the buoy and the profiler are separated by about 5 km; Fig. 1) to enable computation of the bulk fluxes. Here we bin the SEPTR temperature data into 0.5-m bins, and use the upper bin (with a mid-depth of 0.25 m) to represent SST. SEPTR data were acquired from 15 to 26 June 2007, which defines the limits of the flux comparison. For the model–data comparison of SST, we show the ocean model temperature defined in the middle of the uppermost 0.5-m-thick grid cell (i.e., temperature at 0.25 m) for the CAO and UO runs. Because of the lack of radiative flux data at this location, we do not calculate the diurnal cool skin/warm layer effects that were shown for ODAS. As discussed above, the cool skin/warm layer adjustments from 0.25 m to the surface were rather small at ODAS; however, at the METEO site the observed winds were typically weaker than at ODAS (Fig. 5) leaving open the possibility that METEO would have a shallower trapping depth and hence a larger warming in the top 0.25 m than at ODAS.

a. SST at the SEPTR site

The SEPTR SST data are compared against model data in Fig. 11a. Even with only ~4-hourly sampling, the diurnal cycle of SST is clear in the SEPTR data (black line). In addition, the nighttime SST rises from just above 22°C on 16 June to about 24°C on 25 June, with most of the rise occurring between 15 and 19 June (when winds were fairly calm; Fig. 5b). The CAO run SST (blue line in Fig. 11a, representing 0.25-m temperature) shows similar features, except that it is too cold in the first few days (by about 1°–1.5°C), and possibly has a larger diurnal range (this does not appear to be due to the shorter, 1-h sampling interval in COAMPS, as seen by viewing Fig. 12a where both datasets are shown at the same sampling interval).

In general the SST provided by NCODA (Fig. 11a, red line) and by the 2-km high-resolution satellite analysis dataset (Fig. 11a, crosses) are cooler than the SEPTR observations and the coupled model SST, typically by 1° to 2°C. NCODA SST has a maximum difference on 18 June of over 4°C (NCODA minus SEPTR SST), which is due to the imposition of an erroneous cool eddy near the coast on 18–20 June (discussed in more detail in Allard et al. 2010).[5]

As at ODAS, more information on the ability of the coupled model to simulate the diurnal warming can be gained from viewing the vertical temperature change and comparing with the SEPTR profiles. From Figs. 11b,c) it can be seen that the diurnal warming magnitude is up to 1°C in model and observations, at depths of 1–4 m, with similar magnitude to that seen at ODAS (Figs. 8a,b). In both model and observations the temperatures return to the foundation value before sunrise. There is a steep salinity increase of at least 0.5 practical salinity unit (psu) from the surface to 5 m on some days (in model and observations, not shown)[6]: in the model this compensates for the effect of temperature increasing with depth on certain days (e.g., 18 June, Fig. 11c).

It is clear from comparing Figs. 7a and 11a that NCODA is showing an SST significantly lower than the foundation temperatures from SEPTR, while at ODAS, NCODA SST is typically similar to, or warmer than, the ODAS 1-m bulk temperature and the likely foundation temperature. This suggests that NCODA does not have a systematic bias relative to foundation or bulk temperature, and instead has spatial variations in its error characteristics. This is explored further in section 6.

b. Fluxes at the coastal METEO site

This section presents an analysis of the near-surface atmospheric variables measured at the METEO site and

[5] Note that the satellite analysis data shown as circled crosses in Fig. 10 occur on days of significant cloud cover near the coast, when the analysis tends to smooth out coastal features and hence is likely of poor quality. This probably also explains the erroneous NCODA data on these days.

[6] This salinity gradient was quite clear in SEPTR and the model runs and may be due to the freshening influence of the local Magra and Arno rivers. (NCOM includes river input.)

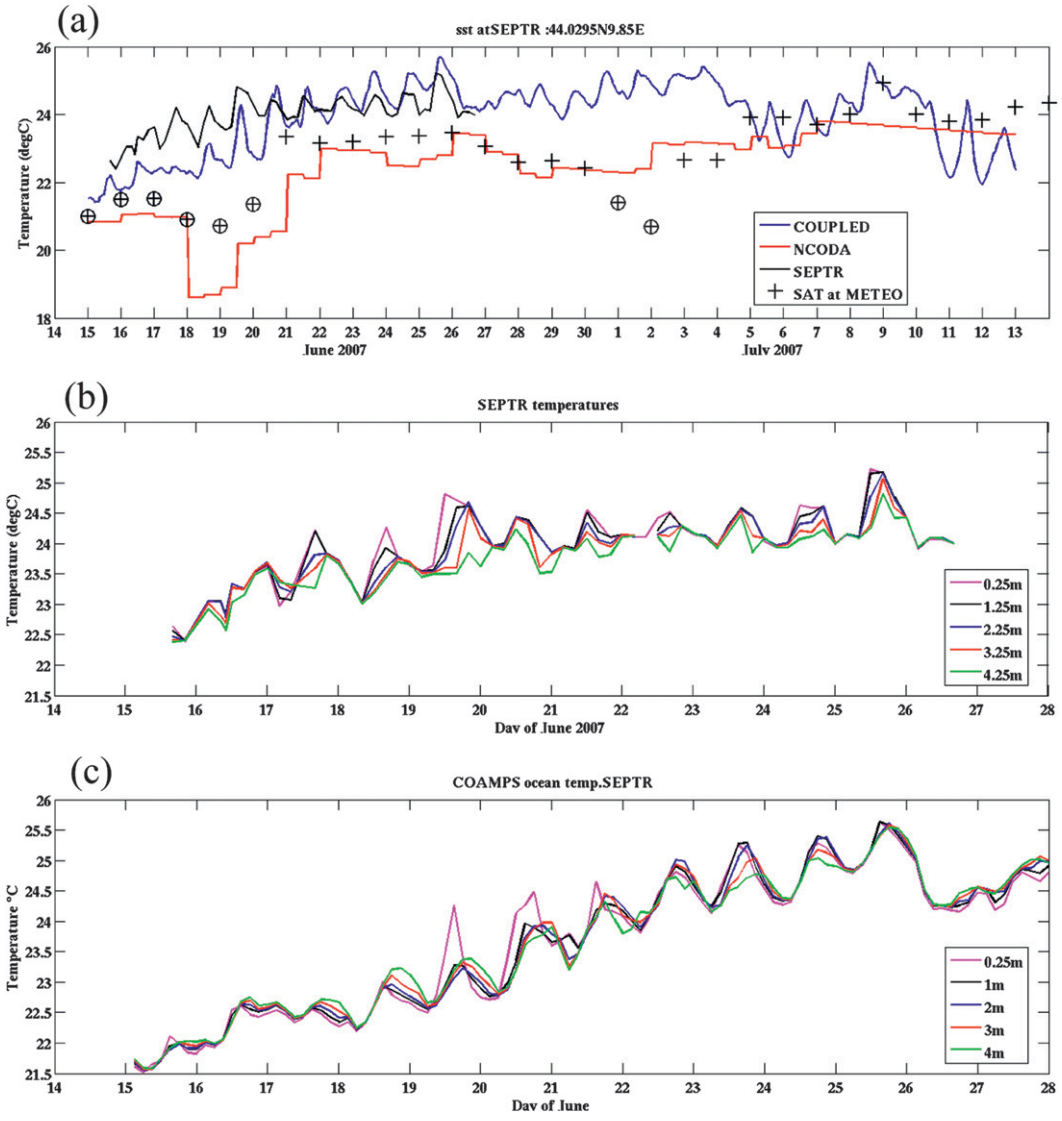

FIG. 11. (a) SST at the LASIE07 coastal location. (black line) The 0.25-m temperature from the SEPTR instrument. (blue line) The 0.25-m coupled model temperature at the nearest grid point to SEPTR. (red line) NCODA SST analysis at the nearest grid point to SEPTR. (crosses) SST analysis from the Medspiration product, for the nearby METEO location. Circled crosses are likely poor quality data (see the text). (b) Near-surface temperature data from the SEPTR instrument. Different colors denote different depth cells, as noted in the legend. (c) The near-surface temperatures from the NCOM component of the coupled model at the nearest grid point to the SEPTR location. Note the different time range in (b) and (c) relative to (a).

of the fluxes derived from these quantities combined with the SST from the SEPTR datasets. Figure 12b shows the 2-m air temperatures from the METEO buoy and the model, both sampled at the times of SEPTR profiles: for comparison the SST for the same data range and at the same sampling intervals is shown in Fig. 12a. The 2-m air temperature from the CAO run is significantly warmer than that in the UA run during the first half of the record, partly because of the erroneous eddy in NCODA discussed above. The CAO air temperature is closer to the observed temperature (Fig. 12b), although it still has a large cool bias up to 20 June, related to the cool bias in SST during those days, relative to SEPTR (Fig. 12a).

Despite the improvement in SST and air temperature in the CAO run with respect to the UA run, the sensible heat flux (Fig. 13a) is not particularly improved in the former run. The coupled model tends to be more unstable than the observations while the uncoupled model is more stable: the mean bias in SST minus 2-m air temperature difference relative to observations is 0.61

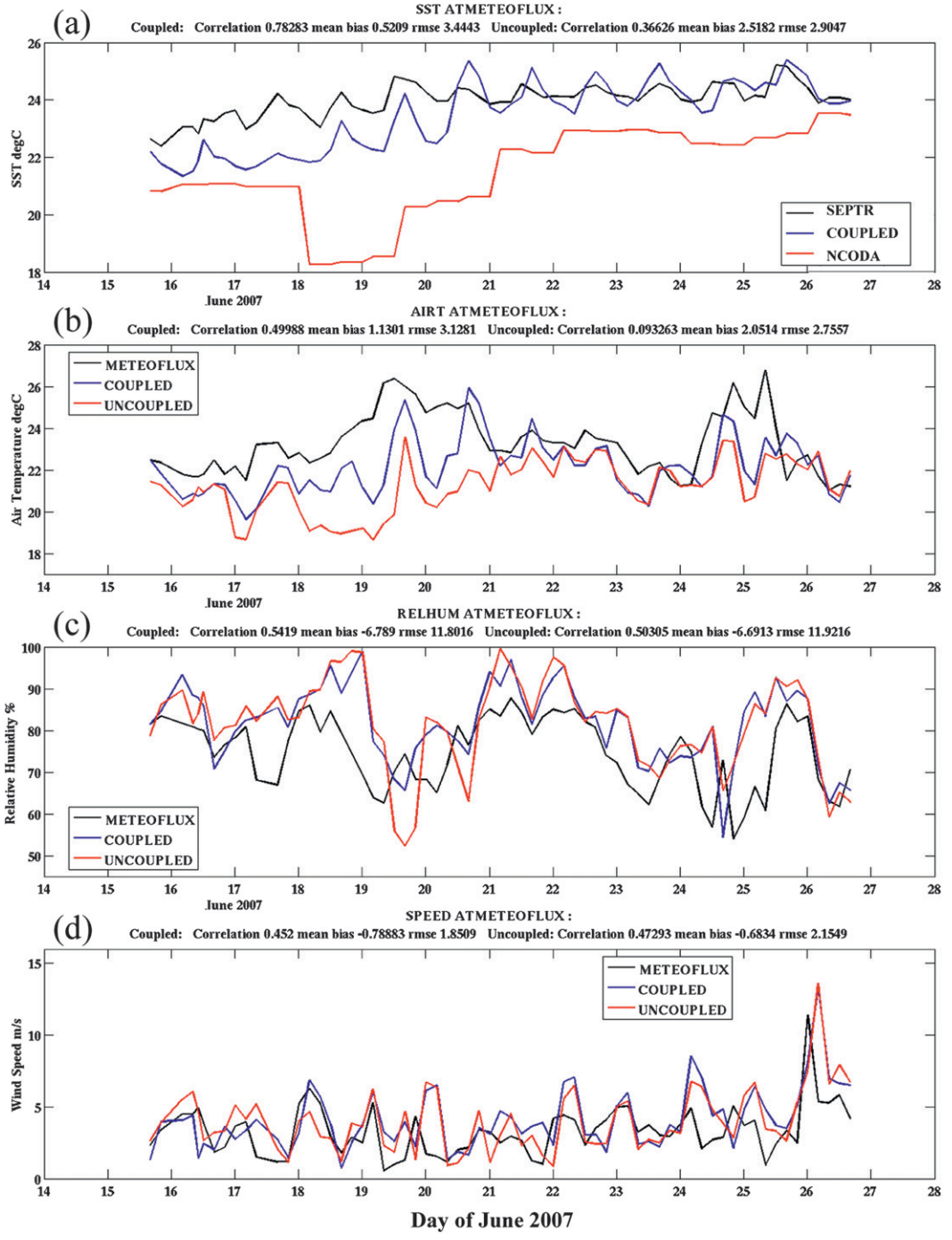

FIG. 12. Time series of variables at the METEO location: observations (black), coupled model (blue), and uncoupled (red). Data from observations and models are sampled about every 4 h. (a) SST (using SEPTR for observed values), (b) air temperature at 2m, (c) relative humidity at 2m, and (d) wind speed at 2m (observations) and 10m (model). METEOFLUX refers to variables or fluxes computed using METEO and SEPTR data and shown for the period of the SEPTR observations.

(model minus observation) for CAO and −0.47 for UA; likewise, the bias in sensible heat flux is similar in magnitude for both cases but opposite in sign (Fig. 13a and Table 2b).

In contrast to the sensible heat flux, the latent heat flux is arguably more directly dependent on absolute SST through its dependence on q_s, the saturation specific humidity at the surface temperature. The q_s is an exponential

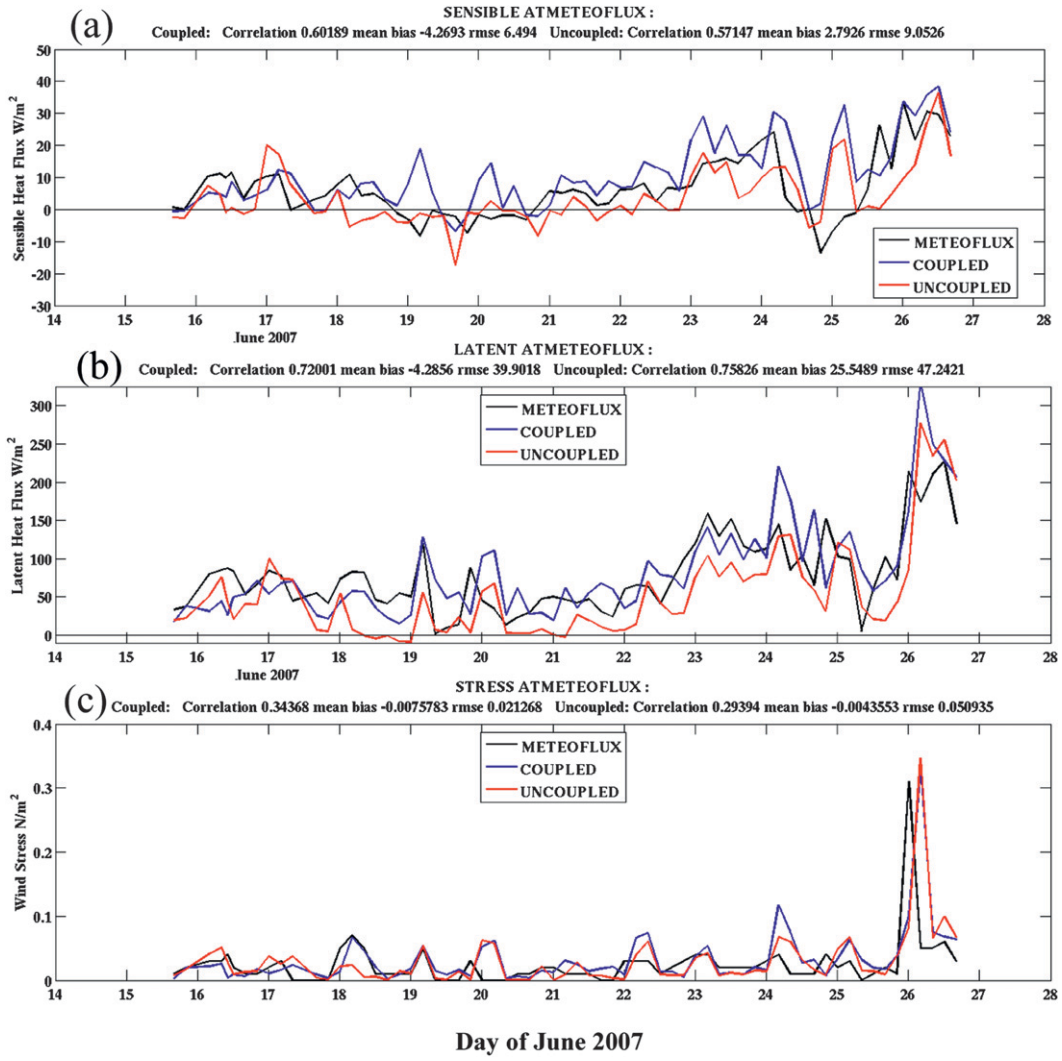

FIG. 13. Time series of fluxes at the METEO/SEPTR location: observations (black), coupled model (blue) and uncoupled (red). (a) Sensible heat flux, (b) latent heat flux, and (c) wind stress. METEOFLUX refers to fluxes computed using METEO and SEPTR data and shown for the period and sampling interval of the SEPTR observations. Data from observations and models are sampled about every 4 h.

function of SST and is significantly biased low in UA because of its cool SST. The CAO latent heat flux is much improved over UA in terms of the mean bias, −4.3 versus 25.6 W m^{-2}, respectively (Fig. 13b and Table 2). Although UA has a slightly higher correlation with observations (0.75 vs 0.72 for CAO), the rmse is higher in UA (Table 2b). The improvement lasts beyond the period of the erroneous eddy (18–20 June).

6. Ocean response to the modulation of fluxes by coupling

In this section we examine in more detail how differences in surface fluxes may affect the oceanic fields of the coupled and uncoupled simulations of the Ligurian Sea.

a. Spatial variability of fluxes

The warm SST at the SEPTR location (relative to the deep water ODAS site) is part of a warm coastal band seen in the observed climatology (see the inset in Fig. 1) and throughout the month long simulation,[7] as seen in the time average of CAO run SST (i.e., 0.25-m temperature) shown in Fig. 14a. As mentioned in the introduction, a frontal zone separates the cool waters of the central Ligurian Sea gyre, with upwelling isopycnals, and exposure to frequent strong winds, from the coastal

[7] In this section we use data for the period 15 June–12 July 2007 (referred to as a "month average" here).

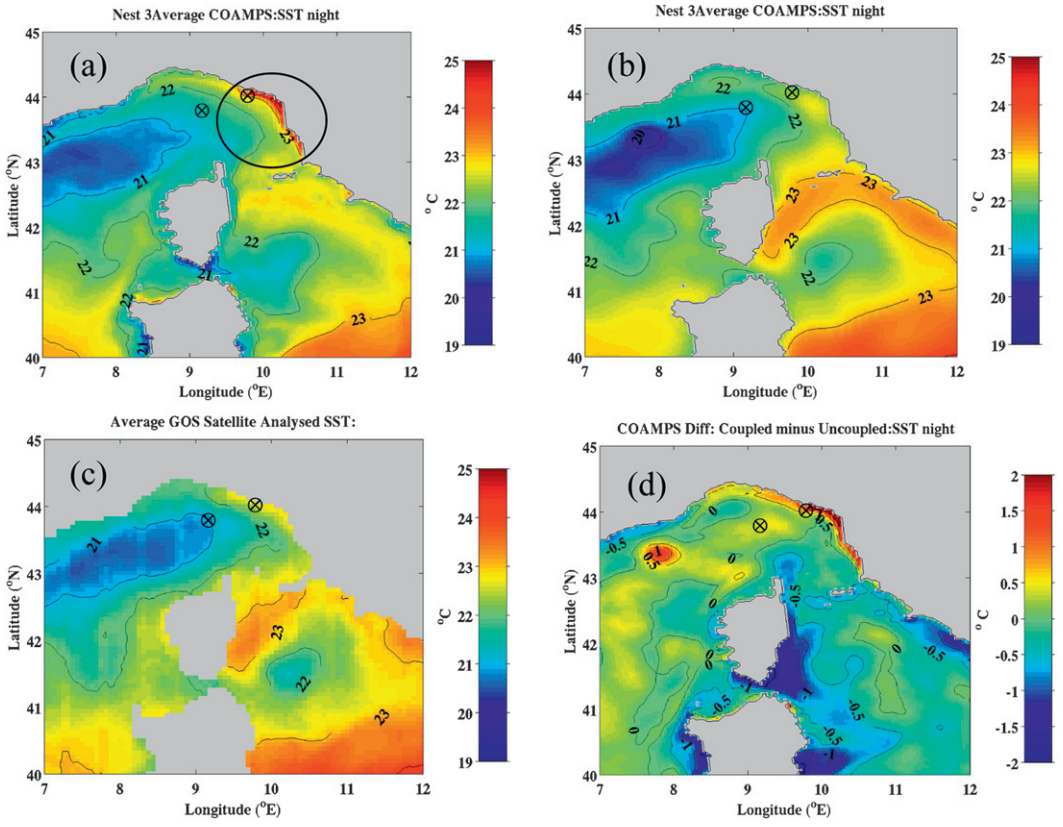

FIG. 14. Month-long (15 Jun to 12 Jul 2007) averages of nighttime SST: (a) from the coupled COAMPS model, (b) from the NCODA analysis, (c) from the GOS CNR product, and (d) the difference between (a) and (b). The coastal area of interest is circled in (a).

region, where weaker winds, strong solar insolation, and shallow bathymetry are conducive to warming of the near-surface ocean. The warm band occurs in the northeast Ligurian Sea and Tyrrehnian Sea, including off La Spezia and farther south toward Pisa, Italy (area circled in Fig. 14a). The corresponding time average from NCODA (Fig. 14b) shows a much weaker feature near the coast, while the GOS-CNR SST has a coastal temperature signal slightly closer to the coupled model (Fig. 14c). The difference between the time-averaged CAO SST and NCODA SST reaches up to 2°C in the narrow coastal band[8] (Fig. 14d). As discussed above, the LASIE07 in situ data show that the CAO run is better at representing near surface temperature than NCODA in this coastal region.

To investigate in detail the effect of coupling on ocean model SST evolution, we need to look at the total heat flux into the ocean and how that is modified by coupling. The total heat flux comprises sensible and latent turbulent heat fluxes and net longwave and shortwave radiative fluxes, all at the surface (we use the convention that positive total heat flux means the ocean loses heat). The month-long average of total heat flux in the coupled run is negative everywhere (not shown), meaning the ocean is gaining heat, because of the very large solar fluxes at this location and time of year. The region where the ocean's heat gain is a minimum is actually in the same coastal zone discussed above, because of the large sensible and latent heat flux out of the ocean. The difference (CAO vs UA) in total heat flux is between 50 and 100 W m^{-2} in this coastal zone (see Fig. 15a), a 50%–100% change relative to the uncoupled model. The major contributor to the heat flux difference was brought by the latent heat (~60% contribution), followed by sensible (~20%) and longwave flux (~10%—note there is a direct effect of SST on the outgoing longwave flux), while the solar insolation contribution was small and not spatially coherent with the coastal feature. There are also enhancements in the wind stress in the coastal zone in the CAO run: they reach nearly 25% of the value modeled in the UA case (Fig. 15b).

[8] The differences are not a result of diurnal warming because of the selection of nighttime data only in Fig. 14.

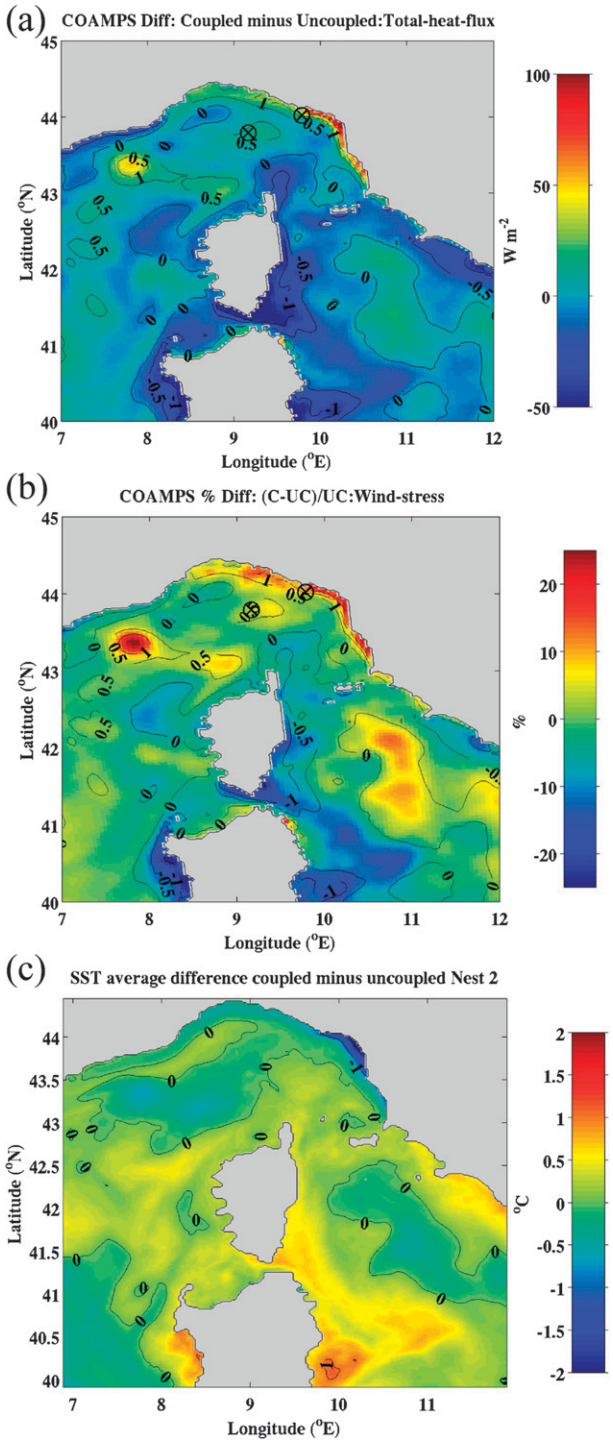

FIG. 15. (a) The difference between coupled and uncoupled model for total heat flux averaged over a month. (Positive values of total heat flux difference denote ocean losing more heat in the coupled model.) (b) The percentage difference between coupled and uncoupled model for wind stress. (c) Difference in 1-month-average SST for the coupled model minus uncoupled ocean model.

b. *Response of the ocean surface and mixed layer*

An estimate of the effect of the total heat flux change on SST can be made as follows. Assuming a mixed layer depth H, over which all the surface heat flux is distributed, the temperature change ΔT averaged over the mixed layer in time Δt due to surface heat fluxes is given by

$$\Delta T = \frac{Q\Delta t}{H\rho c_p},$$

where Q is time-averaged total heat flux, ρ is ocean density, and c_p is the specific heat capacity of water.

The difference δT in temperature change between the CAO and UO ocean components in time Δt, is then given by

$$\delta T = \frac{\delta Q\Delta t}{H\rho c_p}, \tag{1}$$

where δQ is the difference in total heat flux between CAO and UA. For reference, typical mixed layer depths from the model (CAO and UO) near the ODAS location were 10 m (cf. 10–20 m deduced from LASIE07 CTDs; Allard et al. 2010). At the METEO/SEPTR location a true mixed layer was generally not present, but the extent of influence of the surface fluxes at can be estimated as the vertical extent of diurnal warming at SEPTR, which was between 5 and 10 m (not shown). Using values of $\delta Q = 50$ W m^{-2} from Fig. 15a, and approximating $\rho = 1000$ kg m^{-3} and $c_p = 4000$ J kg^{-3}, a typical mixed layer depth of $H = 10$ m gives $\delta T \sim 3.2$°C from (1). The corresponding estimate for $H = 20$ m is 1.6°C and that for $H = 5$ m is 6.4°C. These estimates can be compared with the difference in month-average SST from the ocean model used in the CAO and UO simulations, which reaches up to 1°–2°C of cooling in the coastal zone of interest (see Fig. 15c), close to that given by (1) when H is at the large end of its range (i.e., $H =$ 20 m). However, the difference in month-average SST does not exactly correspond to (1), which is the difference (coupled minus uncoupled) in SST *change* over the length of the run. Computation of this latter quantity showed the values reach 3°C of cooling in the LASIE07 coastal area (not shown), consistent with $H = 10$ m. However, this difference field is more affected by transient features than the month-long average, and does not show such strong correspondence with Fig. 15a. The spatial correlation between the heat flux difference (Fig. 15a) and the month-average SST difference (Fig. 15c) is −0.80, which suggests that enhanced surface fluxes are the most likely cause of the change in ocean model SST.

To illustrate and validate the difference between the SST in the CAO run and that in the UO run, we present

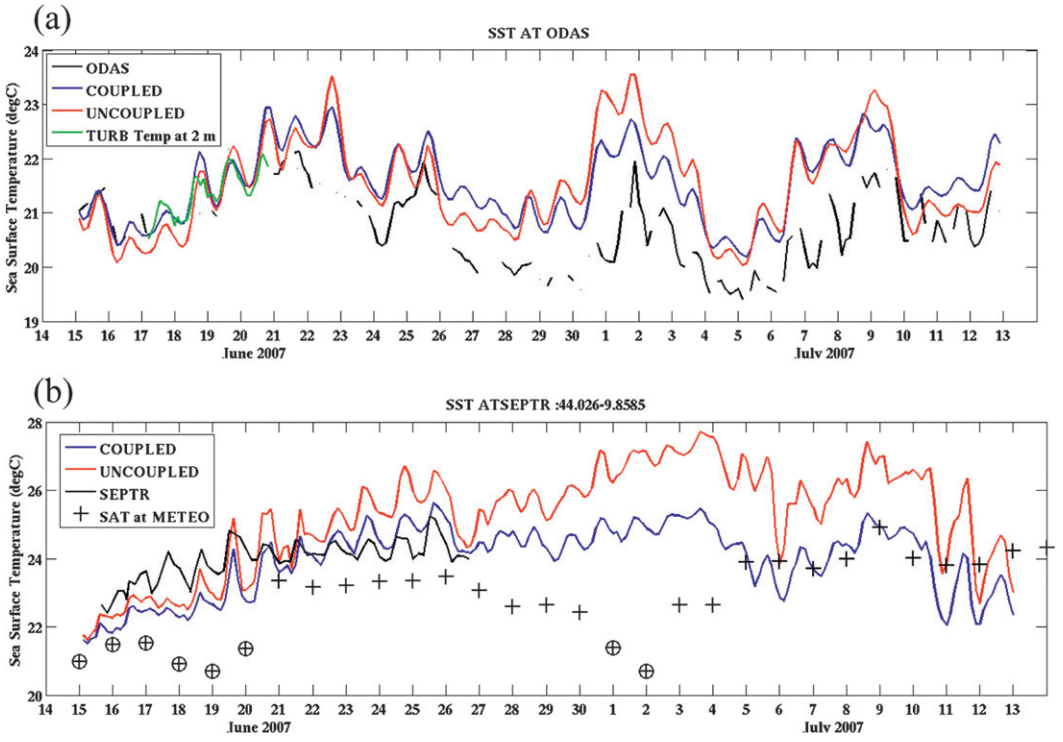

FIG. 16. (a) Time series of SST at the ODAS location. Curves show (see the legend) the ODAS 1-m ocean temperature, the corresponding 1m temperature from the fully coupled run and the uncoupled ocean (UO) run, and 2-m temperatures derived from turbulence probe data. (b) Time series of SST at the SEPTR location. Curves show the 0.25-m temperature from the SEPTR instrument, and the 0.25-m model temperature from the coupled and uncoupled model. Crosses are the SST analysis from the Medspiration product, for the nearby METEO location: circled crosses are likely poor quality data (see the text).

SST time series from both at the ODAS and SEPTR locations discussed above in sections 4 and 5 (Figs. 16a,b, now the red lines show the UO ocean model results). It is immediately apparent that the largest differences between the two model runs occur at the shallow SEPTR location (Fig. 16b): the SST from the UO run can be up to 2°C warmer than the CAO run. In the period up to the 26 June the in situ SEPTR data show that the CAO run is closer to observations than UA.

At ODAS the differences in SST between CAO and UO ocean simulations are not systematic (consistent with Fig. 15c, which shows small differences in this location when averaged over the month), but there is a tendency for the UO run to be too warm during strong diurnal cycle days.

7. Conclusions

The coupled COAMPS model has been validated against in situ and satellite data from the LASIE07 experiment in the Ligurian Sea (northwestern Mediterranean) in the summer of 2007. A month-long simulation was performed, with data assimilation for the atmosphere, for a fully coupled case and an uncoupled case that used an analysis SST to compute bulk fluxes.

When compared against independent (nonassimilated) buoy data, the coupled model wind speeds correlate at 0.60 against a deep-ocean station and 0.43 at a coastal station. At the coastal station, an overestimate of the land breeze in the model led to the smaller correlation. The mean bias between model and observations is less than 1 m s^{-1} at both locations, while the rmse is about 2.5 m s^{-1}.

About 10 days into the run the coupled model SST develops a warm bias at the deep-water station; comparisons with multiple SST data sources confirm the warm error bias of the model, partly due to the underestimation of a strong wind event during 25–27 June. The diurnal cycle of upper-ocean temperature is reasonably well represented by the coupled model at both sites, although the near surface ocean appears to be too stratified at night early in the record at the deep site. Despite the warm SST bias, correlations between the coupled model and observations at the deep-water site for sensible heat fluxes and latent heat fluxes are 0.53 and 0.58, respectively, significant at 99%. The differences between coupled and uncoupled run at the deep-water site are generally small.

Mean biases are about 4 W m^{-2} for sensible and 26–31 W m^{-2} for latent heat flux, with an rmse of 6–8 and 42–57 W m^{-2}, respectively.

At the coastal site the SST in the coupled model is much improved upon the SST analysis (viz., NCODA) used for the uncoupled atmospheric model, which does not resolve a narrow coastal front and inshore warm temperatures. Averaged over 1 month, the coupled model SST is higher than NCODA SST in the coastal LASIE07 zone by up to 2°C, and compares well with in situ observations. Consequently, at the coastal site the latent heat flux is better in the coupled model, particularly in terms of mean bias (-4.3 W m^{-2} in the coupled run vs 25.6 W m^{-2} in the uncoupled). There is a 50%–100% enhancement of combined total heat flux and a 25% enhancement of wind stress in the coupled model in the coastal zone, relative to the uncoupled case. This change in total heat flux affects the SST in the ocean model: averaged over a month, the coupled model SST is 1°–2°C cooler than in an uncoupled ocean run in the LASIE07 coastal zone, and agrees better with observations.

These results from the Ligurian Sea in summer may be compared with, and added to, those of Pullen et al. (2007) and Allard et al. (2010), for the northern Adriatic Sea in winter, who also found that the coupled model provided better heat fluxes in the coastal zone (where the NCODA SST did not resolve a cool coastal current), but not in the interior of the sea. These results should help guide forecasters as to where and when a coupled model provides added value over uncoupled ocean and atmosphere models.

Acknowledgments. The members of the LASIE07 and LIGURE2007 projects are thanked for their willingness to share data and ideas. Particular thanks to Roberto Bozzano and Sara Pensieri, CNR-ISSIA (Italy), for provision of ODAS data; Bruno Buongiorno, CNR-ISAC (Italy), for helpful interpretations of the satellite SST dataset; and Joerg Forster (Forschungsanstalt der Bundeswehr fur Wasserschall und Geophysik, Kiel, Germany) and colleagues for providing data. Alvaro Semedo, University of Upsala (Sweden) is thanked for comments on the ceilometer data; and Michel Rixen (NURC, Italy) for very useful comments on manuscript; Emanuel Coelho (NRL, United States) for early discussions on LASIE07 data and coupled modeling. Rupsi Pal of NRL performed fast and helpful simulations with the GOTM code. Paul Martin, Charlie Barron, Clarke Rowley, Germana Peggion, and Jim Richman of NRL provided useful support and discussion of the results. The Italian CNR is thanked for having made R/V *Urania* available during the dedicated cruise LIGURE2007, and the captain and crew are also thanked for their contributions to making these observations. The activity was partly supported by the "MOM" CNR-RSTL project. RJS, TC, TAS, and RA were supported by the High Performance Computing Modernization Program's Battlespace Environments Institute and NRL's 6.2 Core Program "Coupled Ocean Wave Prediction System" (Program Element PE 0602435N).

REFERENCES

Allard, R. A., and Coauthors, 2010: Validation test report for the Coupled Ocean Atmospheric Mesoscale Prediction System (COAMPS) version 5. Naval Research Laboratory Rep. NRL/MR/7320-10-9283, 172 pp. [Available online at http://www7320.nrlssc.navy.mil/pubs/2010/allard2-2010.pdf.]

Artale, V., and Coauthors, 2010: An atmosphere-ocean regional climate model for the Mediterranean area: Assessment of a present climate simulation. *Climate Dyn.,* **35,** 721–740.

Astraldi, M., and G. P. Gasparini, 1992: The seasonal characteristics of the circulation in the north Mediterranean basin and their relationship with atmospheric-climatic conditions. *J. Geophys. Res.,* **97,** 9531–9540.

——, and ——, 1994: The seasonal characteristics of the circulation in the Tyrrhenian Sea. *Seasonal and Interannual Variability of the Western Mediterranean Sea,* Coastal and Estuarine Studies, P. E. A. Violette, Ed., Vol. 46, Amer. Geophys. Union, 115–134.

Barron, C. N., and A. B. Kara, 2006: Satellite-based daily SSTs over the global ocean. *Geophys. Res. Lett.,* **33,** L15603, doi:10.1029/2006GL026356.

——, ——, P. J. Martin, R. C. Rhodes, and L. F. Smedstad, 2006: Formulation, implementation and examination of vertical coordinate choices in the Global Navy Coastal Ocean Model (NCOM). *Ocean Modell.,* **11,** 347–375.

Barth, A., A. Alvera-Azcarate, M. Rixen, and J.-M. Beckers, 2005: Two-way nested model of mesoscale circulation in the Ligurian Sea. *Prog. Oceanogr.,* **66,** 171–189.

Burchard, H., K. Bolding, and M. R. Villarreal, 1999: GOTM–A general ocean turbulence model: Theory, applications and test cases. Tech. Rep. EUR 18745 EN, European Commission.

Buzzi, A., and A. Speranza, 1983: Cyclogenesis in the lee of the Alps. *Mesoscale Meteorology—Theories, Observations, and Models,* D. K. Lilly and T. Gal-Chen, Eds., D. Reidel Publishing Company, 55–142.

Carniel, S., L. Kantha, A. Bergamasco, H. Prandke, R. J. Small, and M. Sclavo, 2010: Layered structures in the Ligurian sea. *Il Nuovo Cimento B,* **125,** 1567–1586.

Chen, S., and Coauthors, 2003: COAMPS version 3 model description. NRL Publication NRL/PU/7500-03-448, May 2003, 143 pp.

——, T. J. Campbell, H. Jin, S. Gaberšek, R. H. Hodur, and P. Martin, 2010: Effect of two-way air–sea coupling in high and low wind speed regimes. *Mon. Wea. Rev.,* **138,** 3579–3602.

Crépon, M., L. Wald, and J.-M. Monget, 1982: Low frequency waves in the Ligurian Sea during December 1977. *J. Geophys. Res.,* **87,** 595–600.

——, M. Boukthir, B. Barnier, and F. Aikman III, 1989: Horizontal ocean circulation forced by deep water formation. Part I: An analytical study. *J. Phys. Oceanogr.,* **19,** 1781–1792.

Cummings, J. A., 2005: Operational multivariate ocean data assimilation. *Quart. J. Roy. Meteor. Soc.,* **131,** 3583–3604.

Drobinski, P., and Coauthors, 2005: Summer mistral at the exit of the Rhone valley. *Quart. J. Roy. Meteor. Soc.,* **131,** 353–375.

Fairall, C. W., E. F. Bradley, D. P. Rogers, J. B. Edson, and G. S. Young, 1996a: Bulk parameterisation of air-sea fluxes for Tropical Ocean-Global Atmosphere Coupled-Ocean Atmosphere Response Experiment. *J. Geophys. Res.,* **101,** 3747–3764.

——, ——, J. S. Godfrey, G. A. Wick, J. B. Edson, and G. S. Young, 1996b: Cool-skin and warm layer effects on sea surface temperature. *J. Geophys. Res.,* **101,** 1295–1308.

——, ——, J. E. Hare, A. A. Grachev, and J. B. Edson, 2003: Bulk parameterization of air-sea fluxes: Updates and verification for the COARE algorithm. *J. Climate,* **16,** 571–591.

Flamant, C., 2003: Alpine lee cyclogenesis influence on air-sea heat exchanges and marine atmospheric boundary layer thermodynamics over the western Mediterranean during a Tramontane/Mistral event. *J. Geophys. Res.,* **108,** 8057, doi:10.1029/2001JC001040.

Flather, R. A., and R. Proctor, 1983: Prediction of North Sea storm surges using numerical models: Recent developments in the UK. *North Sea Dynamics,* J. Sundemann and W. Lenz, Eds., Springer, 299–317.

Grandi, V., A. Carta, L. Gualdesi, F. deStrobel, and S. Fioravanti, 2005: An overview of SEPTR: Shallow water Environmental Profiler in a Trawl-Safe Real Time Configuration. *Proc. IEEE/OES Eighth Working Conf. on Current Measurement Technology*., Southampton, United Kingdom, IEEE, 142–146.

Harshvardhan, R. Davies, D. Randall, and T. Corsetti, 1987: A fast radiation parameterization for atmospheric circulation models. *J. Geophys. Res.,* **92,** 1009–1016.

Herbaut, C., F. Martel, and M. Crépon, 1997: A sensitivity study of the general circulation of the western Mediterranean Sea. Part II: The response to atmospheric forcing. *J. Phys. Oceanogr.,* **27,** 2126–2145.

Hodur, R. M., 1997: The Naval Research Laboratory's Coupled Ocean/Atmosphere Mesoscale Prediction System (COAMPS). *Mon. Wea. Rev.,* **125,** 1414–1430.

Hogan, T. F., and T. E. Rosmond, 1991: The description of the U.S. Navy Operational Global Atmospheric Prediction System's spectral forecast model. *Mon. Wea. Rev.,* **119,** 1786–1815.

Kain, J. S., and J. M. Fritsch, 1993: Convective parameterization for mesoscale models: The Kain-Fritsch scheme. *The Representation of Cumulus Convection in Numerical Models, Meteor. Monogr.,* No. 46, Amer. Meteor. Soc., 165–170.

Large, W. G., J. C. McWilliams, and S. Doney, 1994: Oceanic vertical mixing: A review and a model with nonlocal boundary layer parameterization. *Rev. Geophys.,* **32,** 363–403.

Louis, J.-F., 1979: A parametric model of vertical eddy fluxes in the atmosphere. *Bound.-Layer Meteor.,* **17,** 187–202.

Martin, P. J., 2000: A description of the Navy Coastal Ocean model version 1.0. NRL Rep. NRL/FR/7322-00-9962, Naval Research Laboratory, Stennis Space Center, MS, 42 pp.

——, J. W. Book, and J. D. Doyle, 2006: Simulation of the northern Adriatic circulation during winter 2003. *J. Geophys. Res.,* **111,** C03S12, doi:10.1029/2006JC003511.

May, D. A., M. M. Parmeter, D. S. Olsewski, and B. D. McKenzie, 1998: Operational processing of satellite sea surface temperature retrievals at the Naval Oceanographic Office. *Bull. Amer. Meteor. Soc.,* **79,** 397–407.

Mellor, G. L., and T. Yamada, 1982: Development of a turbulence closure model for geophysical fluid problems. *Rev. Geophys.,* **20,** 851–875.

Marullo, S., B. Buongiorno Nardelli, M. Guarracino, and R. Santoleri, 2007: Observing the Mediterranean from space: 21 years of Pathfinder-AVHRR sea surface temperatures (1985 to 2005): Re-analysis and validation. *Ocean Sci.,* **3,** 299–310.

Onken, R., A. R. Robinson, L. H. Kantha, C. J. Lozano, J. P. Haley, and S. Carniel, 2005: Inter-model nesting and rapid data exchange in distributed systems. *J. Mar. Syst.,* **56,** 45–66, doi:10.1016/j.marsys.2004.09.010.

Orlanski, I., 1976: A simple boundary condition for unbounded hyperbolic flows. *J. Comput. Phys.,* **21,** 251–269.

Paulson, C. A., and J. J. Simpson, 1977: Irradiance measurements in the upper ocean. *J. Phys. Oceanogr.,* **7,** 952–956.

Powell, M. D., P. J. Vickery, and T. A. Reinhold, 2003: Reduced drag coefficient for high wind speeds in tropical cyclones. *Nature,* **422,** 279–283.

Price, J. F., R. A. Weller, and R. Pinkel, 1986: Diurnal cycling: observations and models of the upper ocean response to diurnal heating, cooling and wind mixing. *J. Geophys. Res.,* **91,** 8411–8427.

Pullen, J., J. D. Doyle, T. Haack, C. Dorman, R. P. Signell, and C. M. Lee, 2007: Bora event variability and the role of air-sea feedback. *J. Geophys. Res.,* **112,** C03S18, doi:10.1029/2006JC003276.

Reynolds, R. W., and D. B. Chelton, 2010: Comparisons of daily sea surface temperature analyses for 2007–08. *J. Climate,* **23,** 3545–3562.

Rodi, W., 1987: Examples of calculation methods for flow and mixing in stratified fluids. *J. Geophys. Res.,* **92** (C5), 5305–5328.

Rutledge, S. A., and P. V. Hobbs, 1983: The mesoscale and microscale structure and organization of clouds and precipitation in midlatitude cyclones. VIII: A model for the "seeder-feeder" process in warm-frontal rainbands. *J. Atmos. Sci.,* **40,** 1185–1206.

Salusti, E., 1998: Satellite images of upwellings and cold filament dynamics as transient effects of violent air-sea interactions downstream from the island of Sardinia. *J. Geophys. Res.,* **103,** 3013–3031.

Schott, F., M. Visbeck, U. Send, J. Fischer, L. Stramma, and Y. Desaubies, 1996: Observations of deep convection in the Gulf of Lions, northern Mediterranean, during the winter of 1991–92. *J. Phys. Oceanogr.,* **26,** 505–524.

Sempreviva, A. M., and Coauthors, 2010: Observed development of the vertical structure of the marine boundary layer during the LASIE experiment in the Ligurian Sea. *Ann. Geophys.,* **28,** 17–25.

Smagorinsky, J., 1963: General circulation experiments with the primitive equations. 1: The basic experiment. *Mon. Wea. Rev.,* **91,** 99–164.

Somot, S., F. Sevault, M. Deque, and M. Crepon, 2008: 21st Century climate change scenario for the Mediterranean using a coupled atmosphere-ocean regional climate model. *Global Planet. Change,* **63,** 112–126.

Teixeira, J., 2007: Ligurian Sea Air-Sea Interaction Experiment (LASIE) trial plan. NATO Undersea Research Centre, La Spezia, Italy, 30 pp.

Umlauf, L., and H. Burchard, 2003: A generic length-scale equation for geophysical turbulence. *J. Mar. Res.,* **61,** 235–265.

Wentz, F. J., and D. K. Smith, 1999: A model function for the ocean-normalised radar cross-section at 14 GHz derived from NSCAT observations. *J. Geophys. Res.,* **104,** 11 499–11 514.